The E3 ligase Poe promotes Pericentrin degradation

Brian J. Galletta[a,†], Ramya Varadarajan[a,†], Carey J. Fagerstrom[a], Bing Yang[b], Karen Plevock Haase[a], Katherine McJunkin[b], and Nasser M. Rusan[a,*]

[a]Cell and Developmental Biology Center, National Heart, Lung, and Blood Institute, and [b]Laboratory of Cellular and Developmental Biology, National Institute of Diabetes and Digestive and Kidney Diseases, National Institutes of Health, Bethesda, MD 20892

ABSTRACT **Centrosomes are essential parts of diverse cellular processes, and precise regulation of the levels of their constituent proteins is critical for their function. One such protein is Pericentrin (PCNT) in humans and Pericentrin-like protein (PLP) in *Drosophila*. Increased PCNT expression and its protein accumulation are linked to clinical conditions including cancer, mental disorders, and ciliopathies. However, the mechanisms by which PCNT levels are regulated remain underexplored. Our previous study demonstrated that PLP levels are sharply down-regulated during early spermatogenesis and this regulation is essential to spatially position PLP on the proximal end of centrioles. We hypothesized that the sharp drop in PLP protein was a result of rapid protein degradation during the male germ line premeiotic G2 phase. Here, we show that PLP is subject to ubiquitin-mediated degradation and identify multiple proteins that promote the reduction of PLP levels in spermatocytes, including the UBR box containing E3 ligase Poe (UBR4), which we show binds to PLP. Although protein sequences governing posttranslational regulation of PLP are not restricted to a single region of the protein, we identify a region that is required for Poe-mediated degradation. Experimentally stabilizing PLP, via internal PLP deletions or loss of Poe, leads to PLP accumulation in spermatocytes, its mispositioning along centrioles, and defects in centriole docking in spermatids.**

Monitoring Editor
Yukiko Yamashita
Massachusetts Institute of Technology

Received: Nov 29, 2022
Revised: Jun 7, 2023
Accepted: Jun 13, 2023

INTRODUCTION

Centrosomes, composed of centrioles and the surrounding pericentriolar material (PCM), are the major microtubule organizing centers (MTOCs) in many cells. They serve critical functions including organizing and orienting spindles during cell division, ensuring proper cilia and flagella formation, and many more (Nigg and Raff, 2009; Bettencourt-Dias *et al.*, 2011; Bornens, 2012; Hoffmann, 2021). The proper regulation of the assembly, activity, and disassembly of centrosomes is critical for cellular and tissue function and, as such, for proper organismal development. Defects in these processes can arise through the presence of too few or too many centrosomes, through inactive or overactive centrosomes, and even by changes in suborganellar structure. Therefore, centrosomes must be tightly regulated to ensure that they are intact and functional at the correct time and place (Nigg and Holland, 2018; Schatten and Sun, 2018; Ryniawec and Rogers, 2021).

Significant study of the regulation of centrosomes has focused on regulation of protein–protein interactions, much of which relies on kinases triggering a phosphorylation event that creates or disrupts a protein interaction surface (Conduit *et al.*, 2014; Dzhindzhev *et al.*, 2014; Ohta *et al.*, 2014; Kratz *et al.*, 2015; Woodruff *et al.*, 2015; Wueseke *et al.*, 2016; Boese *et al.*, 2018). Another critical aspect of centrosome protein regulation is ensuring their correct levels at the centrosome or globally throughout the cell (Strnad *et al.*, 2007; D'Angiolella *et al.*, 2010; Arquint *et al.*, 2012; Arquint and Nigg, 2014; Keller *et al.*, 2014) in coordination with the cell cycle. Global protein level regulation is particularly interesting and

This article was published online ahead of print in MBoC in Press (http://www.molbiolcell.org/cgi/doi/10.1091/mbc.E22-11-0534) on June 21, 2023.

†These authors contributed equally to this work and are to be considered as co–first authors.

*Address correspondence to: Nasser M. Rusan (nasser@nih.gov).

Abbreviations used: CHX, cycloheximide; MD, mitochondrial derivative; MTOC, microtubule organization center; PCM, pericentriolar material; PCNT, Pericentrin; PLP, Pericentrin-like protein; RST, round spermatid; SC, spermatocyte; SG, spermatogonia.

complex as it could involve multiple regulatory mechanisms such as transcription, mRNA stability, translation, or posttranslational regulation of the protein itself. A major focus in the area of posttranslational protein level control has been on mechanisms of protein degradation, which is critical for proper centrosome form and function (Zhang and Galardy, 2016; Badarudeen *et al.*, 2022). In fact, inhibition of the proteasome leads to overduplication of the centriole (Duensing *et al.*, 2007), centriole elongation (Korzeniewski *et al.*, 2010), and an even expansion in the PCM (Wigley *et al.*, 1999). More targeted studies in recent years have uncovered many protein degradation mechanisms that control centrosome protein levels both at the centrosome and throughout the cell, including the major centrosome regulatory kinases Plk4/ZYG-1 (Rogers *et al.*, 2009; Holland *et al.*, 2010; Peel *et al.*, 2012; Cunha-Ferreira *et al.*, 2013; Cajanek *et al.*, 2015; Medley *et al.*, 2021) and Polo/Plk1 (Fang *et al.*, 1998; Lindon and Pines, 2004; Braun *et al.*, 2021), and critical centriole proteins such as CP110 (D'Angiolella *et al.*, 2010), STIL/Ana2/Sas-5 (Tang *et al.*, 2011; Arquint *et al.*, 2012; Arquint and Nigg, 2014; Medley *et al.*, 2017), CPAP/Sas4 (Tang *et al.*, 2009), and Sas-6 (Strnad *et al.*, 2007; Puklowski *et al.*, 2011; Badarudeen *et al.*, 2020; Badarudeen *et al.*, 2022). This suggests a tight, multilevel regulation of not only protein activity but also protein availability throughout the cell.

Most of the published protein degradation studies relate to centriole duplication control; considerably less is known about the regulation of PCM proteins by protein degradation. One example that has been studied is the *Drosophila* PCM protein Spd2, global levels of which are under the control of APC/C^{Fzr} (Meghini *et al.*, 2016). The mammalian orthologue of Spd2, Cep192, is also under the control of protein degradation, via SCF^{FBXL13} (Fung *et al.*, 2018). Interestingly, modulating the levels of SCF^{FBXL13} not only tunes the level of Cep192 at the centrosome but also affects the recruitment of gamma-tubulin and the MTOC activity (Fung *et al.*, 2018). It is therefore likely that regulation of other PCM proteins globally is used to regulate MTOC function in the context of the cell cycle or in other cellular circumstances.

Pericentrin (PCNT in humans and Pericentrin-like protein [PLP] in *Drosophila*) is a member of the "bridge" protein class that localizes to the centriole wall and extends into the PCM as a scaffold and regulator of PCM (Varadarajan and Rusan, 2018). Several lines of evidence suggest that regulation of PCNT/PLP levels is critical. PCNT is hyperaccumulated in tumor cells from pancreatic and prostate cancer patients, and it was suggested to be the cause for the characteristic ectopic MTOC formation and microtubule (MT) nucleation in these cells (Sato *et al.*, 1999; Kim *et al.*, 2008). Elevation in PCNT expression has also been reported in patients affected with Down syndrome and bipolar disorders (Anitha *et al.*, 2009; Salemi *et al.*, 2013). Cells harboring trisomy 21 have abnormal PCNT accumulations and defects in cilia formation and function (Galati *et al.*, 2018). Consistent with these observations, artificial elevation of PCNT levels results in defects in MTOCs, abnormal spindles, and aneuploidy (Purohit *et al.*, 1999). Together, all these studies indicate the relevance and the requirement for regulating PCNT level. However, the mechanisms by which the PCNT level is regulated remain unclear. Studies from mammalian cells have shown that PCNT/Kendrin is proteolytically cleaved by PLK1 phosphorylation-dependent Separase activity, in a cell cycle coordinated manner, followed by the degradation of the C-terminal regions of the protein (Lee and Rhee, 2012; Matsuo *et al.*, 2012; Kim *et al.*, 2015). However, the precise mechanisms by which the C-terminus of PCNT is degraded still remain unclear. Interestingly, expression of PCNT (or the related protein AKAP350) truncations results in excess cytoplasmic aggregates, which in turn recruit additional PCM components that nucleate microtubules independent of centrosomes. These studies suggest that regions of PCNT/AKAP350 are required to limit PCM assembly to the proper place and time; however, the regulatory mechanisms that impose these limits remain unexplored (Kolobova *et al.*, 2017; Varadarajan *et al.*, 2017; Jiang *et al.*, 2021).

The *Drosophila* male germ line provides an excellent model for studying the assembly of centrosomes and the regulation of its component proteins. Germ cells undergo a series of amplifying mitoses to produce spermatocytes (SCs) that then enter a prolonged G2 phase. Our previous study demonstrated that the regulation of PLP protein availability during this G2 phase is critical for centriole organization. The position of PLP itself along the centriole is dictated by the timing of its cellular availability during centriole elongation. At the beginning of centriole elongation in SCs, PLP mRNA and protein are available, but as centriole elongation proceeds, both are no longer available, resulting in a restriction of PLP to the most proximal portions of the centriole (Figure 1A; Galletta *et al.*, 2020). This PLP localization at the proximal end dictates the proximal position of PCM. Misexpression of PLP in G2 forces PLP localization to distal positions on the centriole (Supplemental Figure S1A), which drives PCM accumulation in improper distal positions, ultimately resulting in defects in the docking of the centriole to the nucleus in spermatids yielding decapitated sperm (Galletta *et al.*, 2020).

Although some of the PLP protein-level regulation is the result of the timing of transcript availability, we hypothesized that additional regulation at the protein level is also required to precisely control the timing of PLP availability during germ line development, especially to ensure that its levels dramatically drop as the premeiotic G2 proceeds and centrioles elongate. In this study, we demonstrate that PLP is regulated by posttranslational protein degradation in the germ line. In a screen for regulators of PLP positioning along SC centriole, we identified proteins critical for this regulation, including the E3 ligase Poe. Our data indicate that PLP is under multiple levels of regulation to ensure the proper timing of its availability during centriole elongation.

RESULTS AND DISCUSSION

PLP proximal localization is controlled by multiple proteasomal components

Our previous work established that the proximal position of PLP on SC centrioles is dictated by the timing of available PLP protein (Galletta *et al.*, 2020). PLP is available when centrioles are initially built in spermatogonia (SG) and early SCs but not available as the centrioles elongate in premeiotic G2 phase SCs (Figure 1A). We hypothesized that PLP is under strict regulation via degradation to ensure that PLP protein is not available during the centriole elongation period (Figure 1A). To test whether PLP is under degradation–regulation, we monitored PLP levels following drug treatments of cultured *Drosophila* S2 cells. Similar to previous work on PLP (Martinez-Campos *et al.*, 2004; Galletta *et al.*, 2014), we observe multiple bands whose origin (e.g., splice variant, degradation product, etc.) has not been determined. All qualitative and quantitative assessments are made with respect to the highest molecular weight band, which corresponds to the predicted and previously shown PLP size. Consistent with posttranslational regulation via degradation, treatment of S2 cells with cycloheximide (CHX) to block new protein synthesis resulted in a rapid loss of PLP, such that after 6 h PLP was nearly undetectable (Figure 1B, lane 2; Supplemental Figure S1, B and B'). The loss of PLP is not a consequence of a major change in the cell cycle (mitotic index ~6% vs. ~3%; Supplemental Figure S1B''). We then tested whether loss of PLP occurs via

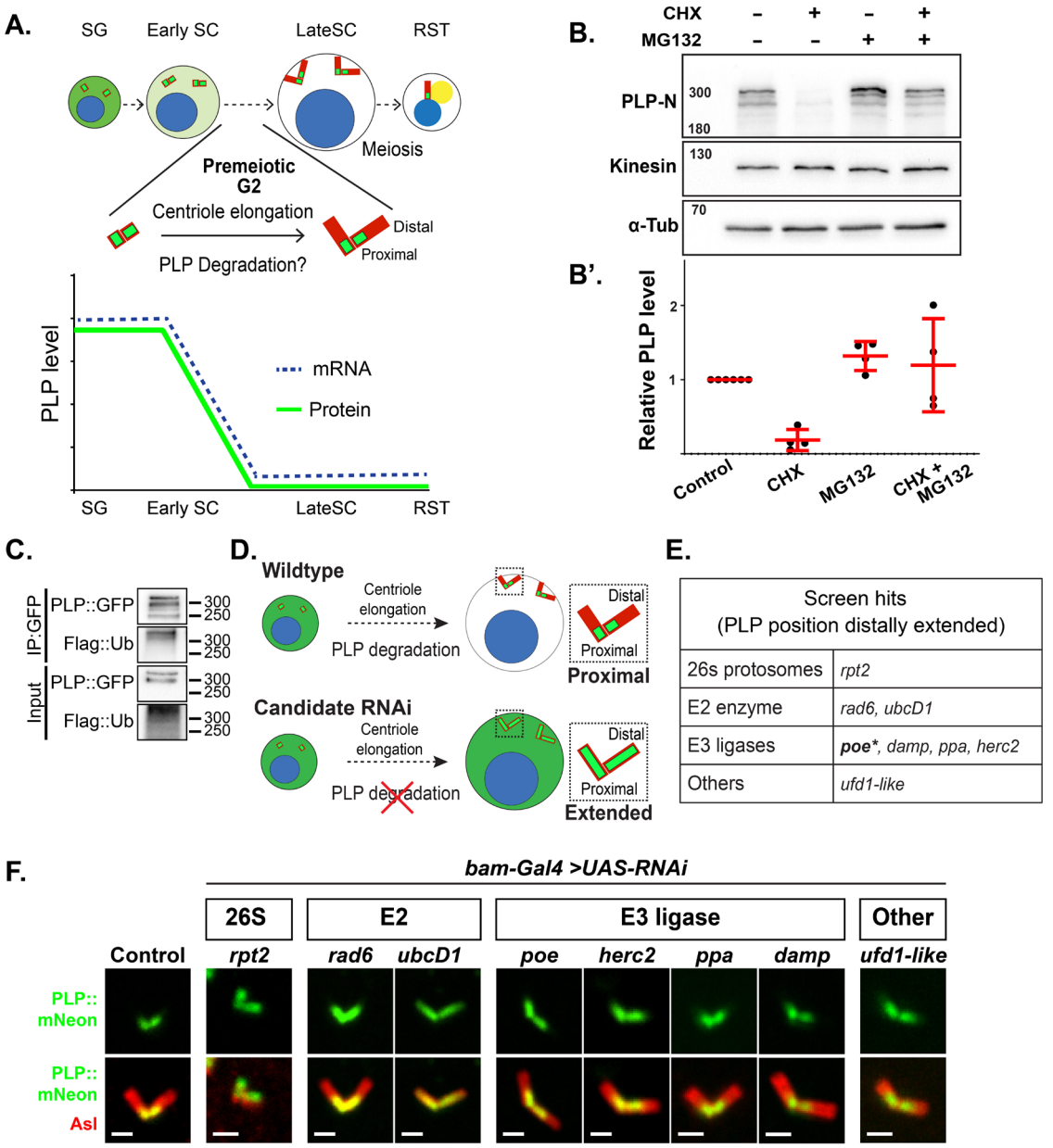

FIGURE 1: PLP levels are down-regulated in developing SCs in a proteasome-dependent manner. (A) Top : Schematic representation of the cytoplasmic and centriole levels of PLP (green) from the end of SG development through SC development and until early spermiogenesis begins. Note that this period includes the premeiotic G2 phase in SC development when centriole elongation occurs. PLP levels are high before centriole elongation and drop as the centriole elongates and thus remains proximal. Centriole (red), Nucleus (blue), mitochondrial derivative (nebenkern; yellow), SG, SCs, and RSTs. Bottom: Graphical representation of the levels of PLP mRNA (blue) and cytoplasmic protein (green) throughout this period showing the drop in both before centriole elongation. (B) Western blot of S2 cell extracts showing endogenous PLP levels under the following drug treatment condition: DMSO—6 h (lane 1), CHX—6 h (lane 2), MG132—6 h (lane3), and dually treated—2 h MG132, followed by 4 h with MG132 and CHX (lane 4). Kinesin and α-tubulin are loading controls. The blots were repeated at least four times. (B') Quantitative analysis of PLP level from blots as in (B). Signals were normalized to kinesin loading control. Values are relative to PLP level in DMSO control. (C) Anti-GFP immunoprecipitation of PLP::GFP (IP::GFP) from S2 cell lysates (input) from cells expressing PLP::GFP and 3X-FLAG-Ubiqutin. PLP is ubiquitinated. This experiment has been repeated three times. (D) Cartoon of RNAi screen rationale. In wild-type cells (top) PLP (green) is actively degraded before centriole elongation leading to its proximal localization on the centriole (red). Upon depletion of a hypothetical regulator of PLP degradation (bottom), PLP cytoplasmic levels do not fall before centriole elongation leading to PLP extended along the centriole abnormally. (E) Genes identified in the RNAi screen to regulate PLP proximal position in SCs. The candidates are grouped into four categories based on function. This study follows up on Poe (bold, asterisk). (F) Position of PLP::mNeon (endogenous tag, green) on centrioles (Asl, red) in late SCs from flies expressing RNAi against the genes in (E), under control of *bam-Gal4*. Control centrioles are from flies carrying *bam*-Gal4 but no RNAi transgene. In all cases, PLP extends further distally on the centriole than in control. Bar = 1 μm. PLP, Pericentrin-like protein; RST, round spermatid; SC, spermatocyte.

a proteasome-mediated pathway by treating S2 cells with the proteasome inhibitor MG132. We found a marginal increase in PLP levels (Figure 1B, lane 3; Supplemental Figure S1, C and C′), which was not due to an MG132-induced mitotic arrest (mitotic index ~6% vs. ~7%; Supplemental Figure S1C″). Finally, we showed that treatment of cells with MG132 prevented the loss of PLP upon treatment with CHX (Figure 1B, lane 4), indicating a significant role of the proteasome in PLP degradation. Consistent with regulation by the proteasome, PLP is subject to ubiquitination in S2 cells (Figure 1C; Supplemental Figure S3B). Together, these data demonstrate that the steady-state levels of PLP in S2 cells are, in part, maintained by a balance of protein production and degradation with a relatively rapid half-life of ~1.1 h.

Having established that PLP levels are under control of the proteasome in S2 cells, we performed an in vivo candidate RNAi knockdown screen of components of the ubiquitin proteasome pathway in developing SCs with the goal of identifying players involved in regulating the proximal/distal position of PLP along the centriole via degradation. Our previous studies on SCs showed that if PLP levels remained high as centrioles elongate, then PLP is found erroneously at more distal positions along the centriole (Galletta *et al.*, 2020; Supplemental Figure S1A). Thus, we hypothesized that loss of a protein required for PLP degradation would elevate PLP levels in SCs during centriole elongation and result in precocious PLP localization beyond the proximal end of the centriole toward the distal end (Figure 1D). We generated a list of 72 candidates (69 were tested) that included a curated selection of genes linked to proteasome degradation. It included components of the 19S/20S proteasome, ubiquitin E2 conjugating enzymes, substrate targeting E3 ligases, and other components associated with protein ubiquitination (Supplemental Table S1). Eight of the E3 ligases included in our list were identified as possible PLP protein-binding partners via an immunoprecipitation (IP) of a fragment of PLP ($PLP^{583\text{-}1810}$) from SF9 cells (*Spodoptera frugiperda*), followed by mass spectrometry (Supplemental Table S2 and S3; six were tested; see *Materials and Methods*). All UAS-RNAi constructs were driven in early spermatogenesis using *bam-Gal4* while endogenous PLP was evaluated using a C-terminal mNeon CRISPR knock in (Galletta *et al.*, 2020). We used a qualitative assessment of PLP position along mature SC using light microscopy to identify gene knockdowns that resulted in distal extension of PLP on centrioles.

Our qualitative screen for extended PLP positioning yielded eight hits (Figure 1E; Supplemental Table S1): three with mild extension of PLP (Damp, Ppa, and Herc2) and five stronger hits that clearly extend PLP (Rpt2, Rad6, UbcD1, Poe, and Ufd1-like). Representative images of PLP position along the centrioles in mature SCs in these eight knockdowns are shown in Figure 1F. In the processes of this qualitative screen, we also noted additional phenotypes from other gene knockdowns such as centriole length abnormalities or formation of PLP cytoplasmic aggregates that were not further studied (Supplemental Table S1). Identifying several E2 and E3 ligases involved in regulating PLP levels in SCs suggests multiple layers of protein degradation regulation act alongside the previously identified mRNA regulation (Galletta *et al.*, 2020). Together, regulation at the level of the mRNA and the protein temporally coordinate the clearance of PLP in the developing SCs to ensure the proximal restriction of PLP. The number of hits in our screen indicates that post-translational regulation of PLP is complex and under the regulation of multiple components of the ubiquitin–proteasome system. This may suggest a degree of redundancy, mechanisms for fine-tuning PLP levels, or the possibility that different regulators modulate PLP function in distinct contexts during germ line development.

Poe regulates PLP levels

We focused on the E3 ubiquitin ligase Poe, which was classified as a strong hit in our screen and was identified by immunoprecipitation-mass specrtometry (IP-MS). Poe is a very large (5322 amino acids [aa]) protein orthologous to the UBR4 (p600) protein in mammals. Both proteins share a small 60-70 aa UBR-box sequence containing a Zn-finger–like motif, termed a "UBR box." This region shares sequence homology with a series of proteins, which have all been linked to degradation of proteins via recognition of specific sequences in their N-termini, termed "N-degrons." Unlike other UBR-box containing proteins, Poe/UBR4 lacks a canonical E3 ligase domain such as a RING, F-box, or HECT domain (Tasaki *et al.*, 2005). Poe/UBR4 has been linked to an incredibly diverse set of processes including protein degradation (Tasaki *et al.*, 2005), spindle orientation (Belzil *et al.*, 2014), meiosis (Sekelsky *et al.*, 1999), male sterility/spermiogenesis (Castrillon *et al.*, 1993; Richards *et al.*, 1996; Fabrizio *et al.*, 1998; Sekelsky *et al.*, 1999), and many others. Although it is a reasonable hypothesis that UBR4/Poe functions in these processes via degradation, this hypothesis remains largely untested.

To better understand how Poe influences PLP, we performed RNAi knockdown of Poe in SCs, followed by detailed fluorescence analysis of PLP. As observed in the screen, knockdown of *poe* showed a significant increase in PLP::mNeon length distally along the centriole in SCs (Figure 2, A and B). The total level of PLP::mNeon protein on the SC centrioles was also increased in Poe knockdown (Figure 2C). Interestingly, however, the density of PLP per unit length remained the same in Poe knockdown compared with controls (Figure 2D), although loss of Poe resulted in an increase of cytoplasmic PLP in SC (Figure 2E). We verified the length, levels, and density measurements using an independently generated stock containing a short-hairpin directed against Poe (Supplemental Figure S2, A–D).

Taken together, these data show that Poe plays an important role in controlling the levels of PLP in SCs. Interestingly, Poe does not appear to play a role in maintaining the steady-state levels of PLP in SG as removal of Poe in SG does not affect PLP levels in these cells (Figure 2E). Thus, Poe influences the distribution of PLP on centrioles by helping limit the availability of the protein during centriole elongation. A simple model is that Poe directly regulates PLP in SC by ubiquitination and targeting it for degradation, but our data do not rule out that Poe could regulate PLP indirectly.

Poe interacts with PLP

In light of the effect of *poe* knockdown on PLP in SCs and the copurification of Poe with PLP in our mass spec screen, we further explored the interaction between PLP and Poe using fragments of PLP and Poe in a yeast two hybrid (Y2H) assay and by coimmunoprecipitation (co-IP) studies. Our Y2H experiments showed that a portion in the central region of PLP ($PLP^{584\text{-}1811}$), the same region used in our pull down for mass spectrometry, interacted with both the N-terminus of Poe ($Poe^{1\text{-}1100}$) and smaller internal fragments of Poe that contain the conserved UBR box, $Poe^{1621\text{-}2040}$ and $Poe^{1741\text{-}1920}$ (Figure 2F). We also tested for interactions by co-IP from S2 cells coexpressing $PLP^{1\text{-}1811}$::GFP and flag-tagged Poe fragments and found that $PLP^{1\text{-}1811}$::GFP co-IPed with $Poe^{1\text{-}1811}$, $Poe^{1101\text{-}2300}$, and $Poe^{3501\text{-}5322}$ (Supplemental Figure S2E) but not $Poe^{2301\text{-}3500}$. Finally, by Y2H we observed an interaction between $PLP^{2539\text{-}2895}$ and $Poe^{1101\text{-}2300}$ (Figure 2F), which we did not further investigate. Overall, while an indirect interaction is possible, our data, particularly the Y2H data, are consistent with a direct PLP–Poe interaction, adding to the evidence that PLP is a potential Poe substrate.

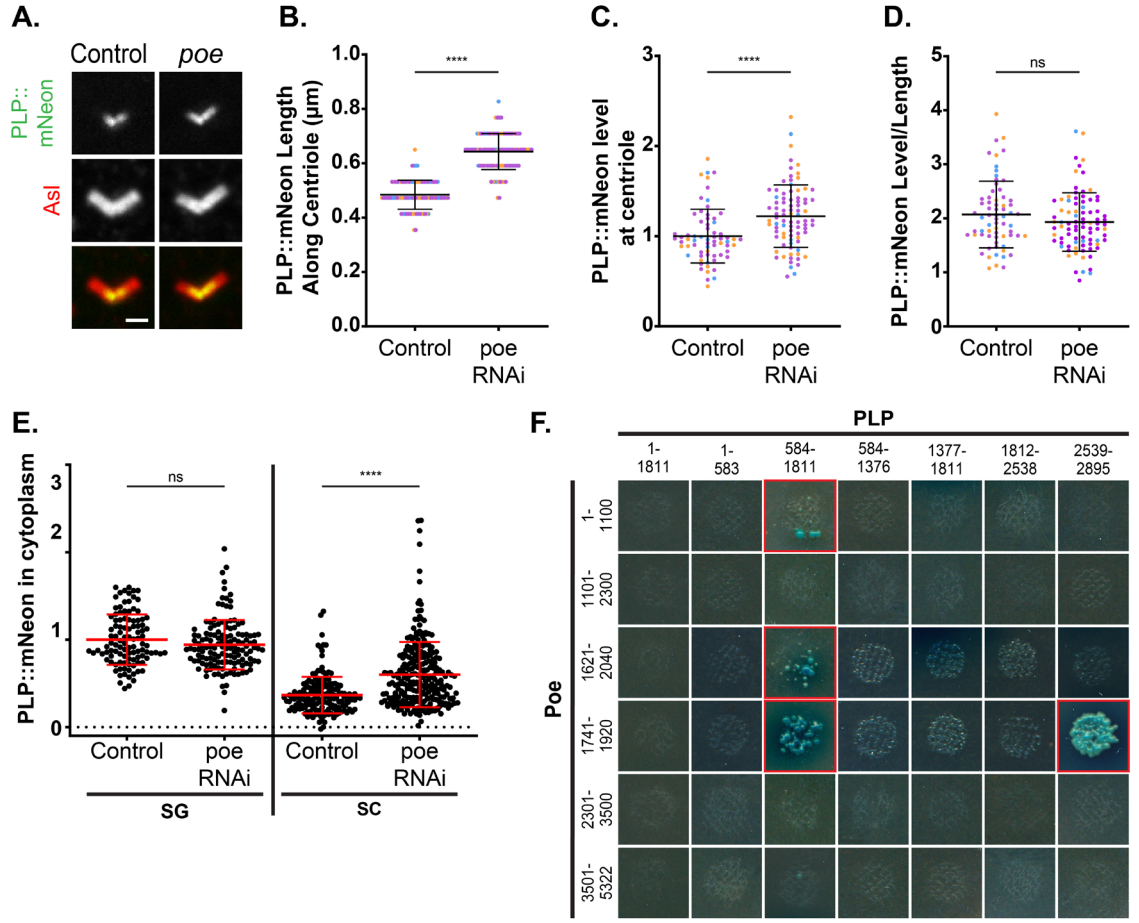

FIGURE 2: Poe regulates PLP centriole position and levels. (A) Position of PLP::mNeon (endogenous tag, green) on centrioles (Asl, red) in late SCs from control flies or flies expressing *poe* RNAi (VDRC# 108296) under control of *bam-Gal4*. PLP extends further distally on centrioles in the knockdown. Bar = 1 µm. (B–D) Measurements of endogenous PLP::mNeon on centrioles for the genotypes as in (A). At least 30 testes of each genotype were examined. Data points from the same trial share the same color. Bar represents the mean ± SD. Statistical comparison by *t* test with Welch's correction when appropriate. **** $p \leq 0.0001$, ns = not significant. (B) Length of PLP::mNeon along late SC centrioles for genotypes as in (A). Measurements along mother centriole only. Control ($n = 65$), *poe* knockdown ($n = 100$). (C) Fluorescent intensity of mNeon on centrioles from RNAi depleted late SCs for genotypes as in (A). The measurements are per centriole and relative to the control level. Control ($n = 67$), *poe* knockdown ($n = 85$). (D) PLP level per unit length along centrioles for genotypes as in (A). Control ($n = 67$), *poe* knockdown ($n = 85$). (E) Cytoplasmic level of endogenous PLP::mNeon measured from SG and late SCs. The individual measurements are shown relative to the cytoplasmic level PLP::mNeon in SG of control. At least 14 testes of each genotype at each stage were measured. Bars represent mean ± SD. Statistical comparison by *t* test with Welch's correction when appropriate. **** $p \leq 0.0001$, ns = not significant. Control (SG, $n = 106$; SC, $n = 176$), *poe* knockdown (SG, $n = 136$; SC $n = 265$). (F) Y2H interaction assay between fragments of PLP (aa indicated) and fragments of Poe (aa indicated). Growth and blue color indicate interaction (red boxes). PLP, Pericentrin-like protein; SC, spermatocyte; SG, spermatogonia.

Multiple regions of PLP are required for proper protein degradation

Having shown that PLP levels are under the control of proteasome-mediated degradation, we tested the hypothesis that PLP is targeted for degradation through specific regions of the PLP protein by assaying the stability of PLP deletion variants in the male germ line (Figure 3A). We generated a series of transgenic animals expressing these deletions under the control of the UAS promoter; note that all variants maintained an intact C-terminal centriole targeting motif (pericentrin-AKAP-450 centrosomal targeting [PACT]). To control the timing of transgene expression, we used the *bam-Gal4* driver, which expresses in early germ line development before centriole elongation, and we have previously shown is sufficient to recapitulate the proximal localization of PLP in mature SCs (Galletta *et al.*, 2020). Western blotting showed that all of the versions of PLP harboring deletions accumulated to a higher steady-state level in the germ line compared with full-length PLP (Figure 3B). Deletion of aa 1-1376 accumulated PLP to much higher levels than deletion of either aa 1-583 or aa 584-1376 alone. This suggests that distinct regulatory elements exist in each of these regions. Further truncation (deletion of aa 1-1811) did not result in further increase in PLP levels, suggesting that most of the post-translational regulation of PLP lies in aa 1-1376. We also examined the cytoplasmic levels of the PLP truncations in the developing male germ line. We found that $PLP^{\Delta 1\text{-}583}$ was elevated in SG and SCs while $PLP^{\Delta 584\text{-}1376}$ was elevated only in SCs (Figure 3C), which is similar to the effect of Poe knockdown (Figure 2E). Codeletion of aa1-583 and aa 584-1376 ($PLP^{\Delta 1\text{-}1376}$) resulted in an even greater increase in cytoplasmic protein amount at both stages measured (Figure 3C).

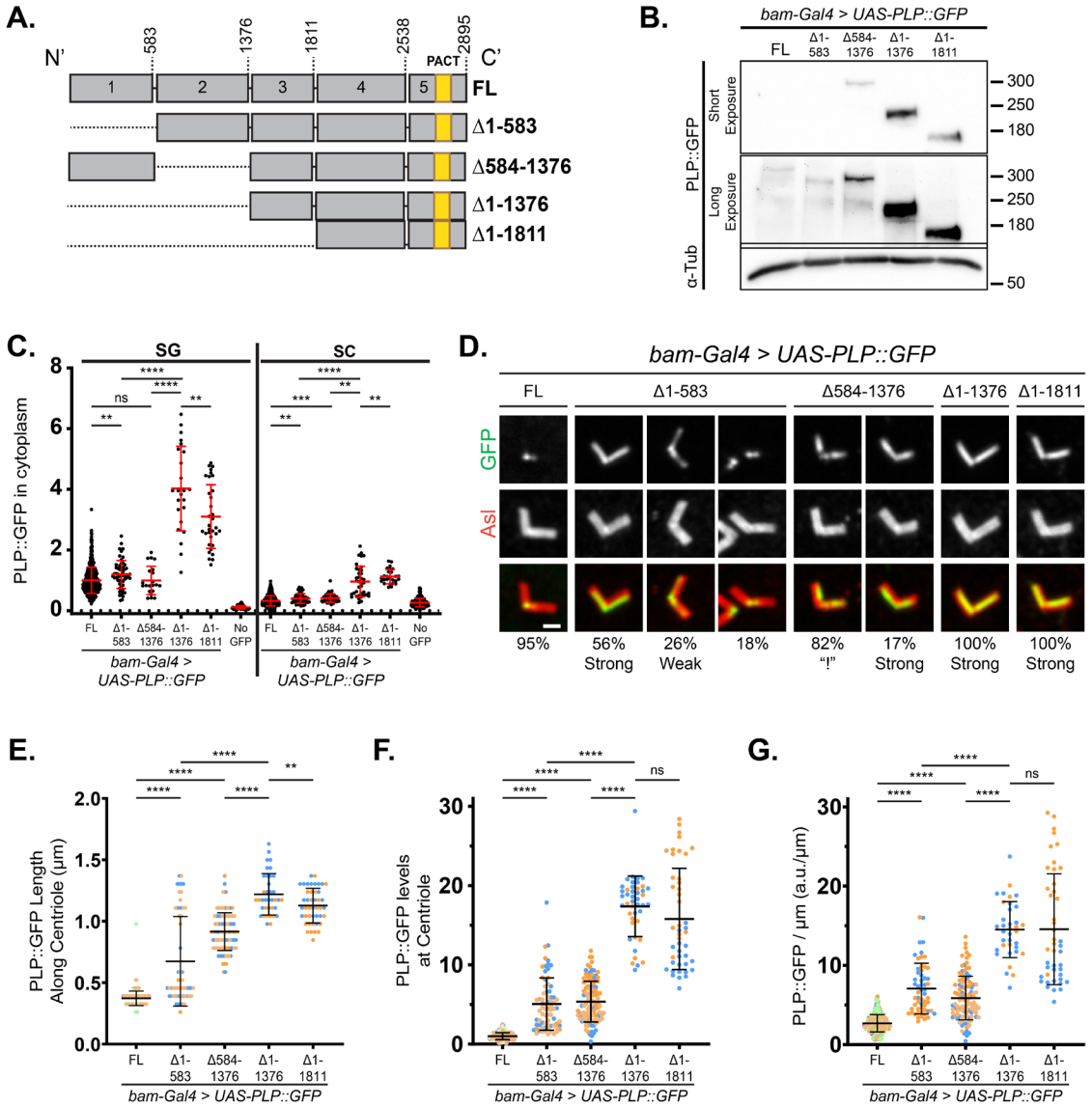

FIGURE 3: Sequences in the N-terminal region of PLP regulate its levels and centriole position. (A) Schematics of PLP deletion constructs. Numbered boxes previously utilized protein subfragments (aa of the most C-terminal residue of the region are indicated), the PACT domain is indicated as a yellow bar. FL represents the PLP-F isoform. Amino acids deleted by each construct are indicated (right). (B) Western blot of testes from indicated genotypes. Anti-GFP antibodies were used to detect PLP. Two different exposures of the same blot are presented to allow visualization of all bands. Some bands contain saturated pixels to allow for visualization of less intense bands. α-tubulin was used as loading control. This experiment was performed at least twice. (C) Cytoplasmic PLP::GFP level in SG and SCs in testes expressing *bam-Gal4>UAS-PLP::GFP* transgenes. "No GFP" measurements were made in *yw* control flies. Measurements are shown relative to the cytoplasmic level of PLP-FL in SG. Cells analyzed: FL (SG, $n = 599$; SC, $n = 1153$), Δ1-583 (SG, $n = 57$; SC, $n = 57$), Δ584-1376 (SG, $n = 21$; SC, $n = 51$), Δ1-1376 (SG, $n = 24$; SC, $n = 38$), and Δ1-1811 (SG, $n = 33$; SC, $n = 26$). Measurements of each cell type were from at least three testes of indicated genotype. (D) Late SC centrioles from flies expressing *bam-Gal4>UAS-PLP::GFP* (green) constructs. Centriole labeled with antibody to Asl (red). Representative images of the distinct localization patterns observed for each genotype are presented and the percentage of centriole pairs showing these localization patterns are indicated below each column. "Strong": robust PLP signal at distal positions, "weak": less robust distal PLP than proximal, "!": resembles exclamation point with dot on proximal end. At least nine testes of each genotype were examined. All deletion constructs show extension of PLP along the entire centriole length. Additional uncommon localizations are shown in Supplemental Figure S3C. Number of centrioles examined: FL ($n = 62$), Δ1-583 ($n = 50$), Δ584-1376 ($n = 112$), Δ1-1376 ($n = 60$), and Δ1-1811 ($n = 45$) Bar = 1 μm. (E–G) Measurements of PLP::GFP on centrioles for the genotypes as in (A). At least nine testes of each genotype were examined. Data points from the same trial share the same color. (E) Length of PLP::mNeon along late SC centrioles for genotypes as in (A). PLPΔ584-1376 occasionally had discontinuous signal along the centriole and the value presented is the sum total length of PLP coverage along the centriole. Measurements along mother centriole only. Measurements made: FL ($n = 316$), Δ1-583 ($n = 57$), Δ584-1376 ($n = 107$), Δ1-1376 ($n = 37$), and Δ1-1811 ($n = 44$). (F) Fluorescent intensity of mNeon on centrioles from RNAi depleted late SCs for genotypes as in (A). The measurements are per centriole and

To confirm that the increases in protein levels were not the result of transgene mRNA differences, we performed quantitative reverse transcription-polymerase chain reaction (RT-PCR). Although we did see a slight elevation of mRNA levels (Supplemental Figure S2, F and G), these levels do not account for the elevated protein levels. For example, PLP$^{\Delta 1\text{-}1376}$ shows dramatically more protein than PLP$^{\Delta 584\text{-}1376}$ although there is no difference in mRNA levels (Figure 3, B and C vs. Supplemental Figure S2, F and G). This result is consistent with S2 cell transfections using truncation constructs of identical concentrations that produce varying levels of PLP protein (Supplemental Figure S3A). In addition, we show that both PLP$^{\Delta 1\text{-}583}$ and PLP$^{\Delta 584\text{-}1376}$ are ubiquitinated in S2 cells (Supplemental Figure S3B), indicating that neither region is the exclusive site of ubiquitination. Together, these data indicate the regulation of PLP degradation is dispersed throughout the first half of the protein, supporting the possibility that PLP levels are regulated via more than one mechanism, as suggested by our SC screen.

We next examined whether the stabilization of PLP caused by these deletions would expand PLP's position distally along the centriole in SCs. Full length (FL) *PLP* (*PLP^{FL}*) driven by *bam-Gal4* localized only to the centriole proximal end (Figure 3D, column 1) similar to the endogenous protein. This indicates that the timing of *PLP* mRNA expressed by the *bam* promoter is sufficiently similar to the endogenous *PLP* promoter, which results in normal centriole localization of the FL protein. Unless otherwise noted, all subsequent experiments were performed using UAS transgenes driven by *bam-Gal4*. PLP$^{\Delta 1\text{-}583}$ or PLP$^{\Delta 584\text{-}1376}$ resulted in PLP localizing to positions beyond the proximal end of the centriole (Figure 3, D and E; Supplemental Figure S3C). Interestingly, PLP$^{\Delta 1\text{-}583}$ and PLP$^{\Delta 584\text{-}1376}$ had distinct distributions/patterns along the centriole. PLP$^{\Delta 1\text{-}583}$ localization was extended distally in 82% of centrioles (Figure 3D; 56% "strong" + 26% "weak"). In contrast, 99% of PLP$^{\Delta 584\text{-}1376}$ centrioles showed distal extension (Figure 3D; 17% "strong" + 82% resembled an exclamation point "!"; the dot on the proximal end). Among other possibilities, these varied distributions may suggest subtle differences in the rate of PLP degradation and/or loading, differences in centriole elongation rates throughout the premeiotic G2 phase, or simply could be an unexpected by-product of the Gal4→UAS expression system. Nonetheless, aa1-583 and aa584-1376 of PLP contain sequences that dictate the distribution and levels of PLP on centrioles (Figure 3, E and F). Interestingly, codeletion of aa1-583 and aa 584-1376 (PLP$^{\Delta 1\text{-}1376}$) resulted in a more consistent and even distribution of PLP localization along the entire centriole (100% "strong"; Figure 3D), consistent with aa1-583 and aa584-1376 containing distinct, nonoverlapping regulatory sequences. Finally, we measured the amount of PLP per unit length on centrioles and observed that unlike Poe KD, both PLP$^{\Delta F1}$ and PLP$^{\Delta F2}$ deletions increased PLP density (Figure 3G).

Collectively, our results indicate that the first 1376 aa of PLP contain major regulatory sequences required for controlling protein level and that deletion of these regulatory regions increased PLP in the cytoplasm, which in turn increased centriolar PLP levels and expanded PLP position along the distal end of centrioles. As discussed previously, this is similar to what is seen when portions of the PLP-related protein AKAP are deleted, which results in accumulation of the protein in cytoplasmic clusters that organize MTs (Kolobova *et al.*, 2017; Varadarajan *et al.*, 2017). Although the mechanism of this regulation remains unclear, the trend in the PLP/PCNT/AKAP family to have multiple regions regulating their functions supports a model for the need of tight regulation of their functions, likely through additional mechanisms beyond Poe function.

Poe acts via the central region of PLP

Thus far, we have shown that loss of Poe elevates PLP levels, that Poe interacts with PLP by Y2H, and that several regions of PLP are required to maintain its own low levels during centriole elongation in SCs. We hypothesized that these three observations are linked such that Poe, in fact, requires specific regions of PLP to regulate its levels. We tested this hypothesis by using a genetic epistasis approach. We combined PLP$^{\Delta 1\text{-}583}$ or PLP$^{\Delta 584\text{-}1376}$ with Poe knockdown and examined the effect on PLP in SCs. Poe knockdown in cells expressing PLP^{FL} resulted in extension of PLP to 1.1 µm as compared with non-RNAi controls showing PLP length of 0.4 µm (Figure 4, A and B). In Poe knockdown cells, PLP$^{\Delta 1\text{-}583}$ showed an average length of 1.3 µm as compared with 0.7 µm in non-RNAi control (Figure 4, A and B). Thus, loss of Poe greatly enhances the PLP$^{\Delta 1\text{-}583}$ phenotype, indicating that Poe likely does not function via PLP aa1-583. In contrast, Poe knockdown in cells expressing PLP$^{\Delta 584\text{-}1376}$ resulted in an average PLP length of 0.9 µm, nearly identical to PLP$^{\Delta 584\text{-}1376}$ in non-RNAi control (Figure 4, A and B). Thus, loss of Poe does not enhance the PLP$^{\Delta 584\text{-}1376}$ phenotype, strongly suggesting that Poe regulates PLP degradation via PLP aa 584-1376.

Interestingly, our result that Poe functions via the more central PLP region of aa 584-1376 suggests a non–N-end rule function for Poe/UBR. There is precedence of such a function in a recent study showing that the Poe orthologue UBR4 did not require its N-end rule UBR box to function secretory protein trafficking (Hegazi *et al.*, 2022). Although our data show a possible N-end rule–independent mechanism of degradation, it should be noted that the mammalian orthologue of PLP, PCNT, is cleaved by Separase and the resulting C-terminal fragment was proposed, but not proven, to be degraded via an N-degron mechanism (Lee and Rhee, 2012; Matsuo *et al.*, 2012). To date, however, no reports have shown an involvement of Separase in centriole disengagement or PLP cleavage in *Drosophila*, and in our current study, we see no clear evidence of PLP cleavage in our experiments. Also, our current study focuses on the degradation of PLP during the extended G2 in SCs that precedes meiosis, whereas the studies of PCNT show the activity of Separase during mitotic exit (Lee and Rhee, 2012).

We next hypothesized that the 584-1376 region contains specific regulatory sequences that 1) exclusively bind Poe, 2) contain a Poe degron, or 3) contain residues targeted for ubiquitination. To test this hypothesis, we performed pull-down experiments in S2 cells expressing fragments of Poe (Poe$^{1\text{-}1100}$, Poe$^{\Delta 1101\text{-}2300}$, and Poe$^{\Delta 3501\text{-}53}$, each of which interacted with PLP by Y2H; Figure 2F), all of which still interacted with PLP^{FL}, PLP $^{\Delta 1\text{-}583}$, and PLP$^{\Delta 584\text{-}1376}$ (Supplemental Figure S3, D–F). This suggests that neither of these regions is solely required for PLP/Poe interaction. Of particular interest, the interaction of

relative to the control level. Measurements made: FL (n = 334), Δ1-583 (n = 73), Δ584-1376 (n = 111), Δ1-1376 (n = 44), and Δ1-1811 (n = 45). (G) PLP level per unit length along centrioles for genotypes as in (D and E). Measurements made: FL (n = 316), Δ1-583 (n = 57), Δ584-1376 (n = 107), Δ1-1376 (n = 36), and Δ1-1811 (n = 44). Bars represent the mean ± SD. Statistical comparison by t test with Welch's correction when appropriate. ** $p \leq 0.01$; *** $p \leq 0.001$; **** $p \leq 0.0001$; ns, not significant. FL, full length.

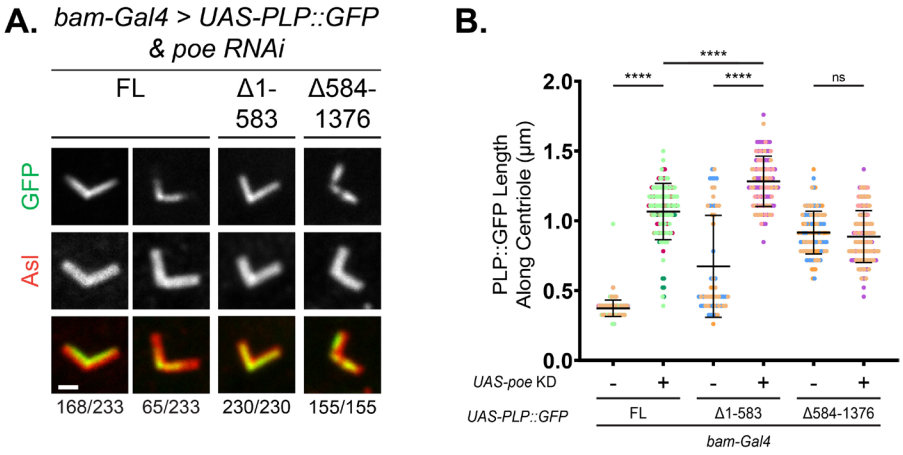

FIGURE 4: Poe promotes PLP degradation via PLP aa 584-1376. (A) Late SC centrioles from flies expressing *bam-Gal4>poe RNAi* and *UAS-PLP::GFP* (green) constructs. Centriole labeled with antibody to Asl (red). Representative images of the distinct localization patterns observed for each genotype are presented, and the number of centriole pairs showing these localization patterns out of the total examined is indicated below each column. At least 30 testes of each genotype were examined. See Figure 3C for examples of *bam-Gal4 > UAS-PLP::GFP* deletions alone. Bar = 1 μm. (B) Length of PLP::mNeon along late SC centrioles for genotypes as in (A). Data points from the same trial share the same color. Data for *bam-Gal4> UAS-PLP::GFP* constructs without RNAi (columns 1, 3, and 5) are reproduced from Figure 3D. PLPΔ584-1376 occasionally had discontinuous signal along the centriole and the value presented is the sum total length of PLP coverage along the centriole. Measurements along mother centriole only. Measurements made: FL and *poe* RNAi ($n = 120$), Δ1-583 and *poe* RNAi ($n = 95$), and Δ584-1376 and *poe* RNAi ($n = 151$). FL, full length; **** $p \leq 0.0001$; ns, not significant.

$PLP^{\Delta 584\text{-}1376}$ with each of the Poe fragments suggests that the genetic interaction between Poe and $PLP^{\Delta 584\text{-}1376}$ (Figure 4) is not a result of Poe binding PLP at aa 584-1376 but rather the loss of a Poe degron or ubiquitination within aa 584-1376.

Posttranslational regulation of PLP is required for centriole/nuclear docking and sperm function

Our previous work showed that mistimed expression of PLP mispositions it along the entire centriole, which causes distal extension of PCM (gamma-tubulin [γ-Tub]), erroneous side-on docking of the centriole to the nucleus, and ultimately a reduction in normal sperm production (Galletta *et al.*, 2020). We therefore examined the consequences of mispositioned PLP resulting from posttranscriptional misregulation on centriole docking and spermiogenesis. Although expression of PLP^{FL} localized properly to the proximal end of centrioles in round spermatids (RSTs, defined as spermatids with a round nuclei and round mitochondrial derivative), PLP carrying the deletions resulted in both PLP and γ-Tub extended distally on centrioles (Figure 5A; Supplemental Figure S4, A and B). Of note, the deletion transgenes, while mispositioned, did not have any effect on the distribution of the endogenous PLP in SCs when the deletions allowed for discrimination of endogenous and exogenous PLP by removing the antibody's epitopes (Supplemental Figure S4C). Thus, the γ-Tub seen at distal positions is directed by the exogenous truncated protein, and the remaining sequences of these PLP transgenes are sufficient for γ-Tub positioning.

We found that the redistribution of PCM by distally extended PLP truncations resulted in erroneous, lateral docking of the centriole to the nucleus (Figure 5, B–D). We were next curious whether knockdown of Poe would also affect centriole docking. Analysis of RSTs in Poe knockdown testes showed many spermatids with multiple centrioles associated with a single, often large, mitochondrial derivative and not always associated with a nucleus (Figure 5E; Supplemental Figure S5A), a phenotype indicative of cytokinesis failing to complete during meiosis (Castrillon *et al.*, 1993). Because mispositioning of PLP alone does not have a profound defect on meiosis (Galletta *et al.*, 2020), this suggests that the meiotic defect in Poe KD SCs results from other, unrelated functions of Poe. Thus, in an attempt to circumvent defects arising from this possible other function, we measured the docking angle of spermatids that received only one centriole and one nucleus, where we found a slight defect in the docking angle of centrioles in the absence of Poe (Figure 5F; *poe*). Thus, our data suggest that Poe has at least two functions during sperm development, 1) a PLP-independent role during meiosis and 2) a PLP-dependent role in centrosome organization and spermatid head–tail docking.

Finally, we examined whether the N-terminal deletions of PLP affected sperm function. We first assayed male fertility and discovered that individual males expressing $PLP^{\Delta 584\text{-}1376}$ showed slight reduction in offspring count, whereas 65% of $PLP^{\Delta 1\text{-}1376}$ and 59% of $PLP^{\Delta 1\text{-}1811}$ males produced no offspring (Supplemental Figure S5B). Consistent with these results, the seminal vesicles (SVs), where mature sperm are stored, were filled with sperm in FL, $PLP^{\Delta 1\text{-}583}$ or $PLP^{\Delta 584\text{-}1376}$ expressing males, but often empty in $PLP^{\Delta 1\text{-}1376}$ or $PLP^{\Delta 1\text{-}1811}$ males (Supplemental Figure S5C). Analysis of testes expressing $PLP^{\Delta 1\text{-}1376}$ or $PLP^{\Delta 1\text{-}1811}$ showed that sperm were formed, but were not motile, explaining the lack of sperm in the SVs (Supplemental Figure S5D). We note that the defect in centriole docking cannot completely explain the defect in sperm motility and male sterility in $PLP^{\Delta 1\text{-}1376}$ and $PLP^{\Delta 1\text{-}1811}$, as $PLP^{\Delta 1\text{-}583}$ and $PLP^{\Delta 584\text{-}1376}$ have similar docking defects (Figure 5, C and D) but are only slightly subfertile and have motile sperm (Supplemental Figure S5, B–D). It is possible that the extremely high protein levels seen in some deletions cause additional effects on sperm formation, motility, or function that do not rely on γ-Tub recruitment.

Collectively, our study shows that PLP is regulated in part via degradation, in particular, in SCs, to ensure the proper distribution of the protein along the length of the centriole. Our genetic epistasis data suggest that the E3 ligase Poe contributes to the degradation of PLP, via aa584-1376 of PLP. Although Poe and its orthologue UBR4 have been linked to the N-end rule pathway of degradation, our data do not support, nor rule out the possibility that Poe regulates PLP via this pathway. However, our genetic epistasis data suggest that during the extended premeiotic G2 of SCs, internal sequences of PLP are more critical for Poe-mediated regulation. Future studies will be required to determine what, if any, contribution N-degron mediated pathways have in PLP degradation in SCs and other cell types. In addition, our co-IP data suggest that these internal sequences of PLP are not required for PLP/Poe to interact, suggesting that these sequences of PLP are instead critical for Poe to exert its influence on PLP levels. Finally, we show that misregulation of PLP levels posttranslationally, via deletion of portions of the protein or loss of Poe, results in defects in spermiogenesis, some of which arise via the mislocalization of PLP along the centriole and the concomitant mislocalization of the PCM.

Although our current study focuses on regulating the availability of the protein in the cytoplasm for assembly onto the centriole during centriole elongation in G2 SCs, we present data in S2 cells that suggest that protein degradation might be used to regulate PLP in other contexts. For example, during spermiogenesis, PLP and other centriole proteins are removed from the centriole, in a process termed "Centrosome Reduction" (Manandhar *et al*., 2005; Schatten and Stearns, 2015; Khire *et al*., 2016). This process of stripping proteins such as PLP (Galletta *et al*., 2020) and Asl (Khire *et al*., 2016) from centrioles is likely subject to tight regulation, possibly via degradation. It also seems likely that regulation of PLP, or other PCM proteins, via degradation might be used in cycling cells to ensure their availability at a precise time during the cell cycle to load onto centrioles and their scarcity at other times. Future studies will tackle these additional biological processes.

MATERIALS AND METHODS

Request a protocol through *Bio-protocol*.

Generation of transgenic flies

A FL PLP (PF isoform) cDNA was used to generate all PLP constructs. The five PLP subfragments were generated previously (Galletta *et al*., 2014). Truncations were generated by PCR of the region of interest (ROI), followed by pENTR/D TOPO cloning. $PLP^{\Delta 584\text{-}1376}$ cDNA was generated as previously described (Lerit *et al*., 2015). cDNAs were cloned into P-element destination vector (pPWG; G = GFP; https://emb.carnegiescience.edu/drosophila-gateway-vector-collection) using the Gateway cloning system (Invitrogen) to express the constructs under the control of a UAS promoter and to include a C-terminal GFP tag. Transgenic flies were generated using standard P-element transformation (BestGene; Chino Hills, CA).

Fly stocks

Flies used in this study were cultured in standard cornmeal–agar media at 25°C. PLP::mNeon is a CRISPR knock in (Galletta *et al*., 2020). Transgenic expression of FL PLP (PLP^{FL}) transgene was used as an experimental control for all PLP truncations. UAS-driven transgenes utilized *bam-Gal4* (Chen and McKearin, 2003) for testes-specific expression in most cases. Where noted, *tubulin-Gal4* (Lee and Luo, 1999) was used for ubiquitous expression. *bam-Gal4*, *tubulin-Gal4*, and RNAi lines (Supplemental Table S1) were obtained from the Bloomington *Drosophila* Stock Center (BDSC) or the Vienna *Drosophila* Resource Center (VDRC). Poe knockdowns utilized VDRC# 108296 (a long hairpin RNAi) for all experiments except those in Supplemental Figure S2, A–D, where BDSC #32945 (a short hairpin RNAi) was used.

Knockdown screen

To identify potential regulators of PLP on SC centrioles, we expressed knockout constructs (Supplemental Table S1) under UAS control using *bam-Gal4* in flies carrying a single copy of the PLP::mNeon CRISPR knock in (Galletta *et al*., 2020). The primary qualitative screen was done in live semisquash testes with Hoechst. Secondary screening was performed in tissues fixed and stained as below. The position of PLP along the centriole was qualitatively assessed. Hits were knockdowns that resulted in PLP qualitatively extending further along the centriole. Other phenotypes observed in developing SCs or spermatids were noted and are presented in Supplemental Table S1.

Plasmids for *Drosophila* S2 expression

PLP expression utilized vectors previously reported (Galletta *et al*., 2014) and contained the same PLP cDNA sequences as the constructs used for expression in flies. For Poe, we first synthesized (Twist Bioscience, South San Fransisco, CA) the cDNA of the following fragments aa1-1100, aa1101-2300, aa1621-2040, aa1741-1920, aa2301-3500, and aa3501-5322 (synthesized in two pieces and then assembled), which were cloned into pENTR/D Topo vector. Destination reactions using the Gateway cloning system (ThermoFisher Scientific, Waltham, MA) were performed to move the cDNA segments into destination vectors containing the Actin5C or Ubiquitin promoter to express protein fragments with the desired tags (AGW, AWG, UWG, UGW, AFHW; G = GFP, F = Flag; https://emb.carnegiescience.edu/drosophila-gateway-vector-collection). AWG-MCS plasmid, expressing GFP alone was used as GFP control for IP experiments. pMT-3xFlag-Ubiquitin was a gift of Greg Rogers.

S2 cell transfection

Drosophila S2 cells (ThermoFisher Scientific and DGRC) were maintained in SF900 media (ThermoFisher Scientific) supplemented with 1× Antibiotic-Antimycotic (ThermoFisher Scientific) or in Schneider's *Drosophila* medium (ThermoFisher Scientific) supplemented with 10% heat-inactivated fetal bovine serum (ThermoFisher Scientific) and 1× Antibiotic-Antimycotic (ThermoFisher Scientific) at 25°C. Cells were transfected using Nucleofection or using Effectene. Nucleofection was performed as recommended by the manufacturer (Lonza, Basel, Switzerland). Approximately 1 µg of plasmid was preincubated in 100-µl nucleofection reagent (50-mM D-mannitol, 15-mM $MgCl_2$, 5-mM KCl, and 120-mM $NaPO_4$, pH 7.2) for 15 min. Plasmid mix was used to resuspend approximately two to five million cells and cells were electroporated using G-030 program in an Amaxa Nucleofector II (Lonza). Transfected cells were then transferred to 2-ml SF900 media and incubated at 25°C for 48–72 h before use. Effectene (Qiagen, Germantown, MD) transfections were performed using 1 µg of plasmid (except pMT-3xFlag-Ubiquitin: 0.5 µg) and 4×10^6 cells as directed by the manufacturer.

Drug treatments. Steady-state PLP protein level was analyzed by treating S2 cells with 50 µM of MG132 or 50 µg/ml of CHX for 6 h. Dimethylsulfoxide (DMSO) without drug was used as control. When both drugs were used, cells were incubated in MG132 for 2 h, followed by CHX and MG132 for 4 h. For transfected cells expressing PLP::GFP, drug treatments were begun 48 h after transfection.

Immunostaining

For tissue. Testes were dissected from 1- to 3-d-old males in Schneider's *Drosophila* (S2) medium (ThermoFisher Scientific) or SF900 media (ThermoFisher Scientific) and then fixed in 4% formaldehyde diluted in PBS for 20–30 min and permeabilized in 1% PBT (triton ×100 diluted in PBS) for 15 min or fixed in 9% formaldehyde in PBS for 20 min, followed by brief washes in 0.3% PBT. Samples were blocked in 5% normal goat serum diluted in 0.3–1% PBT at room temperature for 30 min to 4 h and incubated in primary antibodies diluted in 0.3–1% PBT at the concentration mentioned below, overnight at 4°C. Samples were then washed three times in 0.3–1% PBT, each for 7–10 min and incubated in secondary antibodies diluted in 0.3–1% PBT for 1–2 h at room temperature. After washing and counterstaining with DAPI, the testes were mounted on coverslip using Vectashield (Vector Laboratories, Newark, CA) or Aquapolymount (Polysciences , Warrington, PA). The following are the concentrations of primary antibodies used for immunolabeling in this study: rabbit anti-PLP, raised against the N-terminus region, 1:5000 (Rogers *et al*., 2008); Guinea pig anti-Asl,

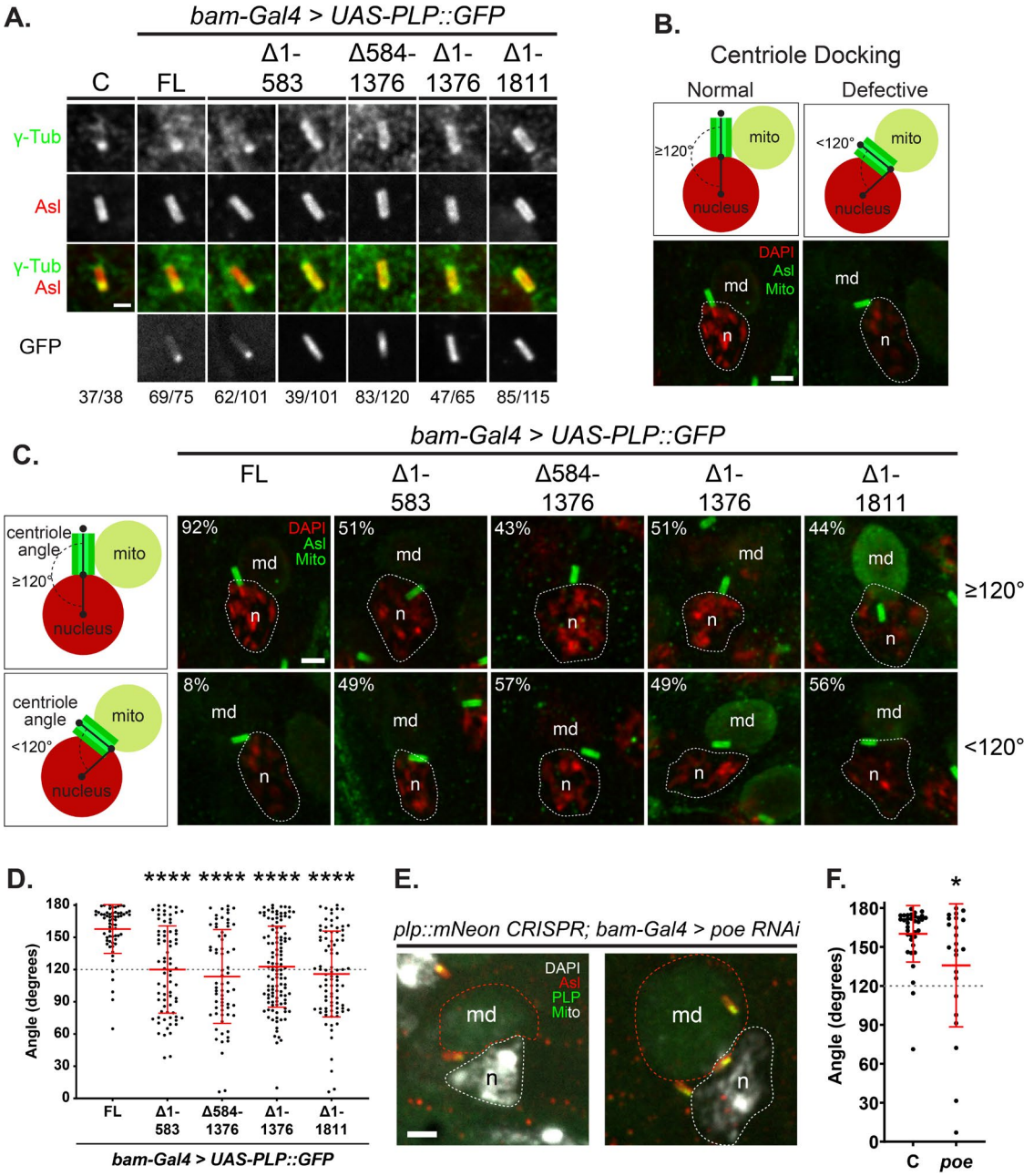

FIGURE 5: Consequences of posttranscriptional PLP misregulation. (A) γ-tubulin localization (γ-Tub, green) on centrioles (Asl, red) from RSTs from flies expressing the indicated *bam-Gal4>UAS-PLP::GFP* constructs (green). GFP is shown in bottom row. Representative images of the distinct localization patterns observed for each genotype are presented, and the number of centriole pairs showing these localization patterns out of the total examined is indicated below each column. Note that the GFP signal in the FL sample is low and there is bleed-through from the Asl signal. Examples of PLP::GFP on centrioles from the genotype without a red fluorophore causing crosstalk in the green channel are shown in Supplemental Figure S4A. At least six testes of each genotype were examined. All deletion constructs show extension of PLP::GFP along the entire centriole length, with $PLP^{\Delta 1\text{-}583}$ showing extension along only ~50% of centrioles. γ-Tub is precociously found along the entire centriole length in PLP truncations, except for $PLP^{\Delta 1\text{-}583}$, which shows γ-Tub along the entire length only in ~50% of centrioles. Additional less common localizations are shown in Supplemental Figure S4B. Bar = 1 μm. (B) Cartoons (top) and RST examples (bottom, DAPI – Red, Asl – green) illustrate proper centriole–nuclear docking (≥120°, left) vs. an incorrect docking (<120°, right). *n* = nucleus, MD = mitochondrial derivative (Nebenkern). (C) Representative images of the position of the centriole (Asl, green) relative to the nucleus (DAPI, red) in RSTs of indicted genotypes. Cartoons (left column) illustrate proper centriole–nuclear docking (≥120°, top) vs. an incorrect docking (<120°, bottom). Angle measurement is indicated with black lines. *N* = nucleus, MD = mitochondrial derivative (nebenkern) The percentage of correct and incorrect docking events for each genotype is indicated (top left corner of each image). The nucleus (n, DAPI, red) is outlined in white. Staining for mitochondria to highlight the MD (green) was performed for some samples. FL (*n* = 64), Δ1-583 (*n* = 74), Δ584-1376 (*n* = 67), Δ1-1376 (*n* = 116), and Δ1-1811 (*n* = 88). At least six testes of each genotype were examined. Bar = 2 μm. (D) Angle of centriole docking in RSTs

TAAATTCGACTCGACTCACGGT	oBY631	Dm gapdh-1 qPCR primer forward
CTCCACCACATACTCGGCTC	oBY632	Dm gapdh-1 qPCR primer reverse
GACGACGGCAACTACAAGACC	oBY641	Dm GFP primer forward
GTTGTACTCCAGCTTGTGCCC	oBY642	Dm GFP primer reverse
CGTATGGAGGAACAGACTCAGC	oBY645	Dm PLP primer forward
CCTCACCCTGGAGTTCATGTAC	oBY646	Dm PLP primer reverse

TABLE 1: Primers used for qPCR:

1:10,000 (Rogers *et al.*, 2008); rabbit anti-Cnn (Galletta *et al.*, 2016); and 1:10,000: mouse γ-Tub (GTU-88; MilliporeSigma, Burlington, MA) 1:500, anti-ATP5A (1:1000, 15H4C4, ab14748; Abcam, Cambridge, UK). Secondary antibodies labeled with Alexa Fluor 488, 568, or 647 conjugations were used in 1:1000 dilution (ThermoFisher Scientific). DAPI (1:1000; ThermoFisher Scientific) was added to secondary antibodies or the second wash after incubation with secondary antibodies.

For S2 cells. Cells were plated on Poly D lysine–coated coverslip and incubated for 30 min. The drug treatments were done by adding CHX or MG132 containing SF900 media at the concentration mentioned earlier and the cells were incubated for 0, 2, 4, or 6 h. Cells were then processed for immunostaining by first removing media, fixing cells in cold 100% methanal for 20 min, briefly washing in 1% PBS containing 0.1% Triton (PBT), blocking in PBT containing 5% goat serum, and incubating in primary antibodies. We used Rabbit anti-phosphorylated Serine 10 Histone 3 antibodies (H3S10P; MilliporeSigma) at 1:1000 dilution and mouse anti-alpha Tubulin (DM1 alpha, MilliporeSigma) at 1:500 dilution. Cells were then washed three times in PBT and incubated in secondary antibodies labeled with Alexa Fluor 488, 568, or 647 conjugations using 1:1000 dilution. Cell were then washed again, labeled for DNA, and mounted using poly Aqua mount. We identified mitotic cells based on the characteristic H3S10P signal from the condensed chromosomes and alpha-tubulin labels of mitotic spindle assembly.

Microscopy

Samples were imaged using a Nikon W1 with a spinning disk confocal head (Yokogawa, Life Science, Tokyo, Japan); 405-, 488-, 561-, and 641-nm laser lines; and Prime BSI cMOS camera (Teledyne Photometrics, Tucson, AZ). Unless noted, images shown in this study were imaged using 100×/1.35 NA silicone immersion objective. Images of testes SV and S2 cells for mitotic index were imaged with 40×/1.3 NA water immersion objective. Cytoplasmic measurements were made with a 40×/1.3 NA oil immersion objective. The microscope was controlled, and images were acquired using Nikon Elements software (Nikon Instruments, Melville, NY). Some images were acquired on an Eclipse Ti2 (Nikon Instruments) with a 100×/1.4NA objective, a CSU-22 spinning disk confocal head (Visitech International, Sunderland, UK), an ORCA-Flash 4.0 CMOS camera (Hamamatsu Photonics, Bridgewater, NJ), and 405-, 491-, 561-, and 642-nm laser lines, controlled by MetaMorph (Molecular Devices, San Jose, CA). All images were analyzed and processed using FIJI (ImageJ; National Institute of Health).

Quantification and statistical analysis

All the data analysis and statistics were performed using Excel (Microsoft) and Prism (Graphpad) software. Statistical analysis was performed using Student's *t* tests with Welch's correction when necessary, or one-way analysis of variance with Dunnett's multiple comparison test, when appropriate. Sample sizes are reported in the figure legends. The mean ± SD is presented.

PLP length along the centriole was measured using ImageJ software from the images of centrioles from the late-stage SCs. Asterless label (Red) was used as a marker to identify these centrioles. Only centrioles with their long axis parallel to the imaging plane were used and only the mother centriole was measured. A line scan was obtained along the length of the centriole. The average intensity of the first and last 10 pixels of the line scan, not on the centriole, was used as background and subtracted from the line scan data. Data were then normalized to the maximum intensity. The number of pixels in the line scan with intensity greater than 50% of maximum was determined, converted to microns, and used as the "PLP length along the centriole." We note that upon precise measurement, PLP expressed under the *bam* promoter occupied slightly less of the proximal end of the centriole (0.38 ± 0.7 μm; Figure 3E) than the knock in construct (0.48 ± 05 μm; Figure 2B). Thus, while the *bam* promoter driving the cDNA is an excellent proxy for endogenous PLP, in particular, its proximal localization, it does not perfectly recapitulate the PLP pattern.

Centriole protein level measurement was performed as described (Galletta *et al.*, 2014). All samples were prepared and then imaged on the same day. Fixed samples were stained with anti-Asl to label centrioles and DAPI to label nuclei. Anti-ATP5A staining was done on some samples to aid in staging spermatids. Sum projections of the entire Z volume of the centriole were generated, an ROI was drawn around the centriole using the Asterless label for reference, and the total integrated density was measured. An identically

from flies expressing *bam-GAL4*>PLP::GFP with the indicated deletions (images in Figure 5C). Dashed line is at 120°. Measurements made: FL ($n = 64$), Δ1-583 ($n = 74$), Δ584-1376 ($n = 67$), Δ1-1376 ($n = 116$), and Δ1-1811 ($n = 88$). Bars are mean ± SD. Statistical comparison to PLP^{FL} by unpaired *t* test with Welch's correction when appropriate. **** $p \leq 0.0001$. (E) Representative images of RSTs from *plp::mneon; bam > poe RNAi* testes showing STs with one centriole/MD (left) vs. >1 centriole /MD (right). DNA (DAPI; gray), Centrioles (Asl; red), PLP (green), and MD (gray and green). (F) *poe* knockdown affects the angle of centriole docking in RSTs. PLP::mneon CRISPR flies express *bam-GAL4* alone (control, C) or *bam-GAL4>poe RNAi* (*poe*). Only RSTs with one centriole per mitochondrial derivative were measured. Measurements made: plp::neon control ($n = 35$), plp::neon, and bam>poe RNAi ($n = 23$). Bars are mean ± SD. Statistical comparison to neon control by unpaired *t* test with Welch's correction. * $p \leq 0.05$. FL, full length.

sized ROI was then used for the background subtraction. The measurements were normalized to the mean value of the *bam-Gal4* control on a given day. This signal was then divided by the number of centrioles present (two or four) so that all data are presented as the signal from one centriole.

Cytoplasmic protein levels were measured in live germ line cells in testes mounted on 50-mm lummox dish (Sarstedt, Numbrecht, Germany) in a drop of S2 media, surrounded by Halocarbon oil 700 (MilliporeSigma) and covered with a No. 1.5 coverslip. Single confocal planes were acquired. Cytoplasmic protein level was analyzed by measuring the average pixel intensity of PLP::mNeon or PLP::GFP in an ROI drawn in the cytoplasm, avoiding any large aggregates or centrosomes. The same ROI was then moved off the sample to acquire a background signal for subtraction. All the measurements were plotted relative to the cytoplasmic level of *bam-Gal4* driving UAS-PLP::GFP in SG on a given imaging day. Because aggregates were avoided, these measurements may underrepresent the total cytoplasmic levels.

PLP level/length was determined by dividing the normalized intensity of PLP on a centriole by the length of PLP along the same centriole.

Immunoprecipitation

For IPs, S2 cells were harvested 2 d after transfection and resuspended in lysis buffer (50-mM Tris, pH 7.2, 125-mM NaCl, 2-mM DDT, 0.1% Triton X-100, 0.1-mM PMSF or 50-mM Tris pH 7.4, 150-mM NaCl, 0.5% Triton X-100, 1-mM DTT, 1-mM PMSF, 1 ug/mL Leupeptin, and 1 ug/mL Pepstatin). After 10–15 min on ice, the lysate was cleared (3 min, 21,130× g, 4°C). The supernatant was then incubated with 15–25 µl of Protein-A Dynabeads conjugated with His-Llama GFP binding protein (GBP [Rothbauer *et al.*, 2008; Patron *et al.*, 2019) for 0.5–2 h at 4°C with mixing. The GFP tagged protein bound to GBP-Dynabeads was washed thrice in lysis buffer on ice, each wash for 1 min, eluted by boiling in 1 or 2× SDS-sample buffer (58-mM Tris pH 6.8, 5% glycerol, 1.95% SDS, 1.55% DTT, 0.05% Bromophenol Blue) for 5–10 min, and analyzed by Western blot. The input lysate and flowthrough were also analyzed.

Western blots

For blots of testes extracts, 50 adult testes were dissected in S2 cell media from 1- to 3-d-old male flies and homogenized in 40 µL of IP lysis buffer, followed by addition of SDS-sample buffer. Samples were boiled for 10 min and stored at –80°C until use. For S2 cells, lysate was prepared by harvesting cells after treatment or transfection, followed by lysing cells in IP lysis buffer, normalizing the volume according to the cell count to achieve similar cells/ml. A small sample was taken, and total protein was estimated by Lowry assay (Lowry *et al.*, 1951). SDS sample buffer was then added, and samples were boiled for 5 min. Volume was adjusted before loading to ensure that the same amount of total protein was loaded into each lane. Samples were run on 6% or 7.5% SDS–polyacrylamide gels. Samples were transferred to nitrocellulose or Polyvinylidene fluoride (PVDF) membrane using Tris-Base Glycine transfer buffer (Novex) with 20% methanol. Blots were blocked in 5% nonfat dry milk diluted in TBST (0.1% Tween 20 diluted in Tris Buffered Saline—50-mM Tris-HCl, pH7.5, 150-mM NaCl) for 30–60 min before incubation with primary antibodies diluted in block overnight at 4°C. Primary antibodies were anti-PLP (N-terminus; 1:5000; Rogers *et al.*, 2008), anti-GFP (JL8; 1:2000–5000; Clontech), anti-alpha-Tubulin (DM1A, 1:10,000; Sigma), anti-Kinesin (SUK4 concentrate; DSHB, 1:2500), anti-Flag (Clone M2; Sigma, 1:2000). Blots were washed in TBST, 0.1% Tween20 diluted in TBS (50-mM Tris-HCl, pH7.5, 150-mM NaCl), the blots were incubated in secondary antibodies conjugated with horseradish peroxidase diluted in TBST (1:2000–10,000; ThermoFisher Scientific). The blots were then washed and detected using SuperSignal West Dura Extended Duration Substrate (Life Technologies) and a ChemiDoc MP Imaging System (Bio-Rad, Hercules, CA).

IP-Mass spectrometry

PLP F2-3 (aa 584-1811) protein was isolated from SF9 insect cells using Bac-to-Bac baculovirus expression system (ThermoFisher). Coding sequence of PLP F2-3 was cloned into pFastBac donor plasmid containing a Flag tag at the C-terminus of the insert site of PLP (gift from Rong Liu, J. Sellers lab, National Heart Lung and Blood Institute, National Institutes of Health, Bethesda, MD). The plasmid was then transformed into DH10Bac *Escherichia coli* cells to allow recombination of PLP-F2-3-Flag with the Bacmid plasmid. The recombinant Bacmid was then transfected into SF9 insect cells, followed by baculoviral infection for large-scale PLP F2-3-Flag amplification. Insect cells expressing PLP F2-3-Flag cDNA were lysed in lysis buffer (50-mM Tris-HCL,7.4, 500-mM NaCl, 1-mM EGTA, 50-µL 0.1M PMSF, 10-µL 5 mg/ml leupeptin, and 50-µL 1M DTT) and 1 tablet of protease inhibitor (Roche, Basel, Switzerland). The lysate was sonicated and then centrifuged at 48,000×g for 30 min at 4°C. The supernatant was then incubated with Flag resin for 2 h at 4°C and then harvested for washes in lysis buffer by centrifugation at 376×g for 2 min. The protein was eluted using elution buffer (50-mM Tris-HCL, 7.4, 100-mM NaCl, and 1-mM EGTA, Flag peptide [GenScript, Piscataway, NJ]; 300 µg/ml). The isolated proteins were then prepared for mass spectrometry using an in-solution protein digestion kit (ThermoFisher Scientific). In brief, the immunoprecipitate was desiccated by Speed Vac (Savant) and resuspended in 50-mM triethylammonium bicarbonate (TEAB), pH 8.0 with 8M urea. Samples were reduced in 20-mM DTT at 37°C for 1 h, alkylated (40-mM iodoacetamide at room temperature for 30 min), and then quenched with DTT to 10 mM. Samples were diluted in TAEB and trypsin digested (~0.1-µg trypsin at 37°C for 24 h). Samples were cleaned with C18 spin columns (MilliporeSigma) as directed by manufacturer before mass spectrometry analysis. Mass spec was performed by the NHLBI Proteomics core facility. Analysis was performed using Scaffold 4 (Proteome Software, Portland, OR).

RNA extraction and qRT-PCR

RNA extraction was adapted from Green and Sambrook (Green and Sambrook, 2020). For each RNA sample, 10 dissected testes tissues were flash frozen in <20 µl of Schneider's *Drosophila* medium and stored at –80°C until RNA extraction. Upon RNA extraction, 100 µl of TRIzol reagent was added in the frozen testes pellet. Samples were then homogenized using disposable plastic pellet pestle for 30 s, followed by addition of 900 µl of TRIzol. Samples were centrifuged at 12,000×g for 10 min at 4°C. The supernatant was then transferred to a fresh tube and incubated at room temperature for 5 min. 200 µl of chloroform was added to the supernatant and the mix was vigorously shaken by hand at room temperature for 15 s and then incubated at room temperature for 2 min. Samples were then centrifuged at 12,000×g for 15 min at 4°C. The upper aqueous phase was transferred to a fresh tube and an equal volume of isopropanol and 1 µL of GlycoBlue Coprecipitant was added to the aqueous phase and mixed gently by inverting. Samples were frozen at –80°C for 30 min and thawed on ice. RNA precipitation was carried out at 20,000×g for 30 min at 4°C. The RNA pellets were then washed twice with 70% ethanol with 5 min of

centrifugation at 4°C. Approximately 8 µl of RNase-free water was added to resuspend the RNA. Quantification of RNA concentration was performed on Nanodrop One. qRT-PCR was performed using the KAPA SYBR Fast One-Step qRT-PCR Kit on QuantStudio 6 Flex Real-Time PCR System using primers in Table 1. Linear dynamic range of the qRT-PCR assay was determined by serial dilution of total RNA. Approximately 25 ng of total RNA was used in each qPCR reaction and three technical replicates were averaged to extract the Ct value for each sample. Data were first normalized to GAPDH and then normalized to levels in *bam-GAL4 > UAS-PLP::GFP*.

Yeast two-hybrid

PLP interactions with E3 ligases were tested using Y2H assay as described (Galletta and Rusan, 2015). In brief, cDNA sequence of PLP and E3 ligases fragments (cloning information above) were cloned to pDEST-pGADT7 (Rossignol *et al*., 2007) and pDEST-pGBKT7-Amp (Galletta *et al*., 2014) using the Gateway cloning system (Life Technologies) and transformed into Y187 and Y2hGold strains, respectively. The transformants were cultured in either SD -Leu or SD -Trp media to select for those carrying the appropriate vector. The strains were mated by mixing Y187 and Y2hGold strains in yeast extract+peptone+dextrose (YPAD) medium overnight with shaking in a flat bottom 96-well plate. Diploids were selected by plating on SD-Leu-Trp dropout media (DDO). Diploids were replica-plated onto test plates: DDO to control for diploid grown and QDO plate (DDO – Ade-Leu-Trp – Ura), DDOXA (DDO + Aureobasidin + X-α-Gal) and QDOXA (DOO – Ade-Leu – Trp –Ura + Aureobasidin A, + X-α-Gal) for interaction tests. Interactions were scored from test plates based on the presence of growth and the development of blue color on the QDOXA plate. Autoactivation was identified by mating to strains carrying empty vectors.

Male fertility

To test male fertility, individual males of the indicated genotypes were crossed to three virgin *yw* females and incubated at 25°C. The number of progeny produced by a single male 12–20 d after crossing was scored. Ten or more males for each genotype were tested. We scored the degree of fertility based on the following criteria (Varadarajan *et al*., 2016): Fertile males produced more than 20 adult progeny; sterile males produced none. Any intermediated phenotypes with < 20 adult progeny or delayed in development were categorized as subfertile males.

Sperm motility in testis

To test whether there were motile sperm in the testis proper, which had yet to migrate to the SV, testes from adult males were dissected and the SV was removed. An insect pin was then used to open the most distal end of the testis and tease out the mature spermatids/sperm in this region. The release of motile sperm was scored by eye. At least 20 testes of each genotype were scored in each of three trials. The percentage of testes with motile sperm was calculated for each genotype and each trial.

Spermatid docking angle

The spermatid docking angle was determined as described (Galletta *et al*., 2020). The angle of centrioles was measured in RSTs (defined as STs with a round nucleus and a mitochondrial derivative with an aspect ratio of <2). Except where noted, RSTs were measured only if there was a normal complement of nuclei and centrioles. RSTs were selected for measurement if the long axis of their centriole was parallel to the imaging plane. Z-projections were taken to include the centriole and the widest point of the nucleus. DAPI staining was used as "the nucleus" in this analysis. An ROI containing all of the nuclear DAPI staining was selected and the centroid was determined using ImageJ. The angle between the centroid of the nucleus, the proximal end of the centriole and the distal end of the centriole, was calculated. If the proximal and distal ends of the centriole could not be determined from PLP signal, the close and far end of the centriole from the DAPI centroid were then used. In these cases, the severity of the angle defect may be underestimated. As previously noted, centrioles with docking errors may be in a different plane than the nucleus and as such overlap in Z-projection. This again may underestimate the angle defect.

Mitotic index calculation

Mitotic index was calculated to estimate the number of mitotic cells resulted during CHX or MG132 treatment conditions. We identified the mitotic and interphase cells based on the H3S10P and DAPI labels. We counted H3S10P-labeled mitotic cells and the total number of cells from the entire field of images. We used ImageJ tools to threshold the images and then automated cell counting. Mitotic index was calculated as a percentage of number of mitotic cells/total number of cells in a field of an image. Each data point in the plot represents the mitotic index of a single image field and the graph includes 6–10 image fields for each treatment conditions. Following is the total number of cells included in this mitotic index estimate: CHX treatment—0 h: 3341, 2 h: 3539, 4 h: 3917, and 6 h: 1877; MG132 treatment—0 h: 4541, 2 h: 4932, 4 h: 2867, and 6 h: 5480.

ACKNOWLEDGMENTS

The authors thank S. Smith, R. Liu, and J. Sellers for help with IP-MassSpec analysis, A. Sodeinde for testes dissections; and R. O'Neill and M. Hannaford for active discussions. They also A. Kelly and T. Akera and their lab members for the critical discussions. The authors thank J. Ryniawec and G. C. Rogers for advising on PLP blots and for reagents and thank the Bloomington *Drosophila* Stock Center and the Vienna *Drosophila* Resource Center for flies and the Developmental Studies Hybridoma Bank for antibodies. The authors thank the NHLBI Light Microscopy, Biophysics, and Proteomics core facilities for technical support. This work was supported by the Division of Intramural Research at the National Institutes of Health/National Heart, Lung, and Blood Institute (1ZIAHL006104 to N.M.R.) and the National Institute of Diabetes and Digestive and Kidney Diseases Intramural Program (ZIADK075147 to K.M.).

REFERENCES

Anitha A, Nakamura K, Yamada K, Iwayama Y, Toyota T, Takei N, Iwata Y, Suzuki K, Sekine Y, Matsuzaki H, *et al.* (2009). Association studies and gene expression analyses of the DISC1-interacting molecules, pericentrin 2 (PCNT2) and DISC1-binding zinc finger protein (DBZ), with schizophrenia and with bipolar disorder. Am J Med Genet B Neuropsychiatr Genet 150B, 967–976.

Arquint C, Nigg EA (2014). STIL microcephaly mutations interfere with APC/C-mediated degradation and cause centriole amplification. Curr Biol 24, 351–360.

Arquint C, Sonnen KF, Stierhof YD, Nigg EA (2012). Cell-cycle-regulated expression of STIL controls centriole number in human cells. J Cell Sci 125, 1342–1352.

Badarudeen B, Anand U, Mukhopadhyay S, Manna TK (2022). Ubiquitin signaling in the control of centriole duplication. Febs J 289, 4830–4849.

Badarudeen B, Gupta R, Nair SV, Chandrasekharan A, Manna TK (2020). The ubiquitin ligase FBXW7 targets the centriolar assembly protein HsSAS-6 for degradation and thereby regulates centriole duplication. J Biol Chem 295, 4428–4437.

Belzil C, Asada N, Ishiguro K, Nakaya T, Parsons K, Pendolino V, Neumayer G, Mapelli M, Nakatani Y, Sanada K, Nguyen MD (2014). p600 regulates

spindle orientation in apical neural progenitors and contributes to neurogenesis in the developing neocortex. Biol Open 3, 475–485.
Bettencourt-Dias M, Hildebrandt F, Pellman D, Woods G, Godinho SA (2011). Centrosomes and cilia in human disease. Trends Genet 27, 307–315.
Boese CJ, Nye J, Buster DW, McLamarrah TA, Byrnes AE, Slep KC, Rusan NM, Rogers GC (2018). Asterless is a Polo-like kinase 4 substrate that both activates and inhibits kinase activity depending on its phosphorylation state. Mol Biol Cell 29, 2874–2886.
Bornens M (2012). The centrosome in cells and organisms. Science 335, 422–426.
Braun AL, Meghini F, Villa-Fombuena G, Guermont M, Fernandez-Martinez E, Qian Z, Martin-Bermudo MD, Gonzalez-Reyes A, Glover DM, Kimata Y (2021). The careful control of Polo kinase by APC/C-Ube2C ensures the intercellular transport of germline centrosomes during Drosophila oogenesis. Open Biol 11, 200371.
Cajanek L, Glatter T, Nigg EA (2015). The E3 ubiquitin ligase Mib1 regulates Plk4 and centriole biogenesis. J Cell Sci 128, 1674–1682.
Castrillon DH, Gonczy P, Alexander S, Rawson R, Eberhart CG, Viswanathan S, DiNardo S, Wasserman SA (1993). Toward a molecular genetic analysis of spermatogenesis in Drosophila melanogaster: characterization of male-sterile mutants generated by single P element mutagenesis. Genetics 135, 489–505.
Chen D, McKearin DM (2003). A discrete transcriptional silencer in the bam gene determines asymmetric division of the Drosophila germline stem cell. Development 130, 1159–1170.
Conduit PT, Feng Z, Richens JH, Baumbach J, Wainman A, Bakshi SD, Dobbelaere J, Johnson S, Lea SM, Raff JW (2014). The centrosome-specific phosphorylation of Cnn by polo/plk1 drives Cnn scaffold assembly and centrosome maturation. Dev Cell 28, 659–669.
Cunha-Ferreira I, Bento I, Pimenta-Marques A, Jana SC, Lince-Faria M, Duarte P, Borrego-Pinto J, Gilberto S, Amado T, Brito D, *et al.* (2013). Regulation of autophosphorylation controls PLK4 self-destruction and centriole number. Curr Biol 23, 2245–2254.
D'Angiolella V, Donato V, Vijayakumar S, Saraf A, Florens L, Washburn MP, Dynlacht B, Pagano M (2010). SCF(Cyclin F) controls centrosome homeostasis and mitotic fidelity through CP110 degradation. Nature 466, 138–142.
Duensing A, Liu Y, Perdreau SA, Kleylein-Sohn J, Nigg EA, Duensing S (2007). Centriole overduplication through the concurrent formation of multiple daughter centrioles at single maternal templates. Oncogene 26, 6280–6288.
Dzhindzhev NS, Tzolovsky G, Lipinszki Z, Schneider S, Lattao R, Fu J, Debski J, Dadlez M, Glover DM (2014). Plk4 phosphorylates Ana2 to Trigger Sas6 recruitment and procentriole formation. Curr Biol 24, 2526–2532.
Fabrizio JJ, Hime G, Lemmon SK, Bazinet C (1998). Genetic dissection of sperm individualization in Drosophila melanogaster. Development 125, 1833–1843.
Fang G, Yu H, Kirschner MW (1998). Direct binding of CDC20 protein family members activates the anaphase-promoting complex in mitosis and G1. Mol Cell 2, 163–171.
Fung E, Richter C, Yang HB, Schaffer I, Fischer R, Kessler BM, Bassermann F, D'Angiolella V (2018). FBXL13 directs the proteolysis of CEP192 to regulate centrosome homeostasis and cell migration. EMBO Rep 19, e44799.
Galati DF, Sullivan KD, Pham AT, Espinosa JM, Pearson CG (2018). Trisomy 21 represses cilia formation and function. Dev Cell 46, 641–650. e6.
Galletta BJ, Fagerstrom CJ, Schoborg TA, McLamarrah TA, Ryniawec JM, Buster DW, Slep KC, Rogers GC, Rusan NM (2016). A centrosome interactome provides insight into organelle assembly and reveals a non-duplication role for Plk4. Nat Commun 7, 12476.
Galletta BJ, Guillen RX, Fagerstrom CJ, Brownlee CW, Lerit DA, Megraw TL, Rogers GC, Rusan NM (2014). Drosophila pericentrin requires interaction with calmodulin for its function at centrosomes and neuronal basal bodies but not at sperm basal bodies. Mol Biol Cell 25, 2682–2694.
Galletta BJ, Ortega JM, Smith SL, Fagerstrom CJ, Fear JM, Mahadevaraju S, Oliver B, Rusan NM (2020). Sperm head-tail linkage requires restriction of pericentriolar material to the proximal centriole end. Dev Cell 53, 86–101. e7.
Galletta BJ, Rusan NM (2015). A yeast two-hybrid approach for probing protein-protein interactions at the centrosome. Methods Cell Biol 129, 251–277.
Green MR, Sambrook J (2020). Total RNA Isolation from *Drosophila melanogaster*. Cold Spring Harb Protoc 2020, 101675.
Hegazi S, Cheng AH, Krupp JJ, Tasaki T, Liu J, Szulc DA, Ling HH, Rios Garcia J, Seecharran S, Basiri T, *et al.* (2022). UBR4/POE facilitates secretory trafficking to maintain circadian clock synchrony. Nat Commun 13, 1594.
Hoffmann I (2021). Centrosomes in mitotic spindle assembly and orientation. Curr Opin Struct Biol 66, 193–198.
Holland AJ, Lan WJ, Cleveland DW (2010). Centriole duplication: a lesson in self-control. Cell Cycle 9, 2731–2736.
Jiang XE, Ho DBT, Mahe K, Mia J, Sepulveda G, Antkowiak M, Jiang LH, Yamada S, Jao LE (2021). Condensation of pericentrin proteins in human cells illuminates phase separation in centrosome assembly. J Cell Sci 134, jcs258897.
Keller D, Orpinell M, Olivier N, Wachsmuth M, Mahen R, Wyss R, Hachet V, Ellenberg J, Manley S, Gonczy P (2014). Mechanisms of HsSAS-6 assembly promoting centriole formation in human cells. J Cell Biol 204, 697–712.
Khire A, Jo KH, Kong D, Akhshi T, Blachon S, Cekic AR, Hynek S, Ha A, Loncarek J, Mennella V, Avidor-Reiss T (2016). Centriole remodeling during spermiogenesis in drosophila. Curr Biol 26, 3183–3189.
Kim J, Choi YL, Vallentin A, Hunrichs BS, Hellerstein MK, Peehl DM, Mochly-Rosen D (2008). Centrosomal PKCbetaII and pericentrin are critical for human prostate cancer growth and angiogenesis. Cancer Res 68, 6831–6839.
Kim J, Lee K, Rhee K (2015). PLK1 regulation of PCNT cleavage ensures fidelity of centriole separation during mitotic exit. Nat Commun 6, 10076.
Kolobova E, Roland JT, Lapierre LA, Williams JA, Mason TA, Goldenring JR (2017). The C-terminal region of A-kinase anchor protein 350 (AKAP350A) enables formation of microtubule-nucleation centers and interacts with pericentriolar proteins. J Biol Chem 292, 20394–20409.
Korzeniewski N, Cuevas R, Duensing A, Duensing S (2010). Daughter centriole elongation is controlled by proteolysis. Mol Biol Cell 21, 3942–3951.
Kratz AS, Barenz F, Richter KT, Hoffmann I (2015). Plk4-dependent phosphorylation of STIL is required for centriole duplication. Biol Open 4, 370–377.
Lee K, Rhee K (2012). Separase-dependent cleavage of pericentrin B is necessary and sufficient for centriole disengagement during mitosis. Cell Cycle 11, 2476–2485.
Lee T, Luo L (1999). Mosaic analysis with a repressible cell marker for studies of gene function in neuronal morphogenesis. Neuron 22, 451–461.
Lerit DA, Jordan HA, Poulton JS, Fagerstrom CJ, Galletta BJ, Peifer M, Rusan NM (2015). Interphase centrosome organization by the PLP-Cnn scaffold is required for centrosome function. J Cell Biol 210, 79–97.
Lindon C, Pines J (2004). Ordered proteolysis in anaphase inactivates Plk1 to contribute to proper mitotic exit in human cells. J Cell Biol 164, 233–241.
Lowry OH, Rosebrough NJ, Farr AL, Randall RJ (1951). Protein measurement with the Folin phenol reagent. J Biol Chem 193, 265–275.
Manandhar G, Schatten H, Sutovsky P (2005). Centrosome reduction during gametogenesis and its significance. Biol Reprod 72, 2–13.
Martinez-Campos M, Basto R, Baker J, Kernan M, Raff JW (2004). The Drosophila pericentrin-like protein is essential for cilia/flagella function, but appears to be dispensable for mitosis. J Cell Biol 165, 673–683.
Matsuo K, Ohsumi K, Iwabuchi M, Kawamata T, Ono Y, Takahashi M (2012). Kendrin is a novel substrate for separase involved in the licensing of centriole duplication. Curr Biol 22, 915–921.
Medley JC, DeMeyer LE, Kabara MM, Song MH (2017). APC/CFZR-1 controls SAS-5 levels to regulate centrosome duplication in *Caenorhabditis elegans*. G3 7, 3937–3946.
Medley JC, DiPanni JR, Schira L, Shaffou BM, Sebou BM, Song MH (2021). APC/CFZR-1 regulates centrosomal ZYG-1 to limit centrosome number. J Cell Sci 134, jcs253088.
Meghini F, Martins T, Tait X, Fujimitsu K, Yamano H, Glover DM, Kimata Y (2016). Targeting of Fzr/Cdh1 for timely activation of the APC/C at the centrosome during mitotic exit. Nat Commun 7, 12607.
Nigg EA, Holland AJ (2018). Once and only once: mechanisms of centriole duplication and their deregulation in disease. Nat Rev Mol Cell Bio 19, 297–312.
Nigg EA, Raff JW (2009). Centrioles, centrosomes, and cilia in health and disease. Cell 139, 663–678.
Ohta M, Ashikawa T, Nozaki Y, Kozuka-Hata H, Goto H, Inagaki M, Oyama M, Kitagawa D (2014). Direct interaction of Plk4 with STIL ensures formation of a single procentriole per parental centriole. Nat Commun 5, 5267.

Patron LA, Nagatomo K, Eves DT, Imad M, Young K, Torvund M, Guo X, Rogers GC, Zinsmaier KE (2019). Cul4 ubiquitin ligase cofactor DCAF12 promotes neurotransmitter release and homeostatic plasticity. J Cell Biol 218, 993–1010.

Peel N, Dougherty M, Goeres J, Liu Y, O'Connell KF (2012). The C. elegans F-box proteins LIN-23 and SEL-10 antagonize centrosome duplication by regulating ZYG-1 levels. J Cell Sci 125, 3535–3544.

Puklowski A, Homsi Y, Keller D, May M, Chauhan S, Kossatz U, Grunwald V, Kubicka S, Pich A, Manns MP, *et al*. (2011). The SCF-FBXW5 E3-ubiquitin ligase is regulated by PLK4 and targets HsSAS-6 to control centrosome duplication. Nat Cell Biol 13, 1004–1009.

Purohit A, Tynan SH, Vallee R, Doxsey SJ (1999). Direct interaction of pericentrin with cytoplasmic dynein light intermediate chain contributes to mitotic spindle organization. J Cell Biol 147, 481–492.

Richards S, Hillman T, Stern M (1996). Mutations in the Drosophila pushover gene confer increased neuronal excitability and spontaneous synaptic vesicle fusion. Genetics 142, 1215–1223.

Rogers GC, Rusan NM, Peifer M, Rogers SL (2008). A multicomponent assembly pathway contributes to the formation of acentrosomal microtubule arrays in interphase Drosophila cells. Mol Biol Cell 19, 3163–3178.

Rogers GC, Rusan NM, Roberts DM, Peifer M, Rogers SL (2009). The SCF Slimb ubiquitin ligase regulates Plk4/Sak levels to block centriole reduplication. J Cell Biol 184, 225–239.

Rossignol T, Logue ME, Reynolds K, Grenon M, Lowndes NF, Butler G (2007). Transcriptional response of Candida parapsilosis following exposure to farnesol. Antimicrob Agents Chemother 51, 2304–2312.

Rothbauer U, Zolghadr K, Muyldermans S, Schepers A, Cardoso MC, Leonhardt H (2008). A versatile nanotrap for biochemical and functional studies with fluorescent fusion proteins. Mol Cell Proteomics 7, 282–289.

Ryniawec JM, Rogers GC (2021). Centrosome instability: when good centrosomes go bad. Cell Mol Life Sci 78, 6775–6795.

Salemi M, Barone C, Romano C, Salluzzo R, Caraci F, Cantarella RA, Salluzzo MG, Drago F, Romano C, Bosco P (2013). Pericentrin expression in Down's syndrome. Neurol Sci 34, 2023–2025.

Sato N, Mizumoto K, Nakamura M, Nakamura K, Kusumoto M, Niiyama H, Ogawa T, Tanaka M (1999). Centrosome abnormalities in pancreatic ductal carcinoma. Clin Cancer Res 5, 963–970.

Schatten G, Stearns T (2015). Sperm centrosomes: kiss your asterless goodbye, for fertility's sake. Curr Biol 25, R1178–R1181.

Schatten H, Sun QY (2018). Functions and dysfunctions of the mammalian centrosome in health, disorders, disease, and aging. Histochem Cell Biol 150, 303–325.

Sekelsky JJ, McKim KS, Messina L, French RL, Hurley WD, Arbel T, Chin GM, Deneen B, Force SJ, Hari KL, *et al*. (1999). Identification of novel Drosophila meiotic genes recovered in a P-element screen. Genetics 152, 529–542.

Strnad P, Leidel S, Vinogradova T, Euteneuer U, Khodjakov A, Gonczy P (2007). Regulated HsSAS-6 levels ensure formation of a single procentriole per centriole during the centrosome duplication cycle. Dev Cell 13, 203–213.

Tang CJC, Fu RH, Wu KS, Hsu WB, Tang TK (2009). CPAP is a cell-cycle regulated protein that controls centriole length. Nat Cell Biol 11, 825–831.

Tang CJC, Lin SY, Hsu WB, Lin YN, Wu CT, Lin YC, Chang CW, Wu KS, Tang TK (2011). The human microcephaly protein STIL interacts with CPAP and is required for procentriole formation. EMBO J 30, 4790–4804.

Tasaki T, Mulder LC, Iwamatsu A, Lee MJ, Davydov IV, Varshavsky A, Muesing M, Kwon YT (2005). A family of mammalian E3 ubiquitin ligases that contain the UBR box motif and recognize N-degrons. Mol Cell Biol 25, 7120–7136.

Varadarajan R, Ayeni J, Jin Z, Homola E, Campbell SD (2016). Myt1 inhibition of Cyclin A/Cdk1 is essential for fusome integrity and premeiotic centriole engagement in Drosophila spermatocytes. Mol Biol Cell 27, 2051–2063.

Varadarajan R, Hammer JA, Rusan NM (2017). A centrosomal scaffold shows some self-control. J Biol Chem 292, 20410–20411.

Varadarajan R, Rusan NM (2018). Bridging centrioles and PCM in proper space and time. Essays Biochem 62, 793–801.

Wigley WC, Fabunmi RP, Lee MG, Marino CR, Muallem S, DeMartino GN, Thomas PJ (1999). Dynamic association of proteasomal machinery with the centrosome. J Cell Biol 145, 481–490.

Woodruff JB, Wueseke O, Viscardi V, Mahamid J, Ochoa SD, Bunkenborg J, Widlund PO, Pozniakovsky A, Zanin E, Bahmanyar S, *et al*. (2015). Centrosomes. Regulated assembly of a supramolecular centrosome scaffold in vitro. Science 348, 808–812.

Wueseke O, Zwicker D, Schwager A, Wong YL, Oegema K, Julicher F, Hyman AA, Woodruff JB (2016). Polo-like kinase phosphorylation determines Caenorhabditis elegans centrosome size and density by biasing SPD-5 toward an assembly-competent conformation. Biol Open 5, 1431–1440.

Zhang Y, Galardy PJ (2016). Ubiquitin, the centrosome, and chromosome segregation. Chromosome Res 24, 77–91.